Review Article

Nano Research
2022, 15(11): 9906–9920

ISSN 1998-0124 CN 11-5974/O4
https://doi.org/10.1007/s12274-022-4379-2

Focus on using nanopore technology for societal health, environmental, and energy challenges

Izadora Mayumi Fujinami Tanimoto[1,2], Benjamin Cressiot[3] (✉), Sandra J. Greive[4], Bruno Le Pioufle[2], Laurent Bacri[1] (✉), and Juan Pelta[1,3] (✉)

[1] *LAMBE, CNRS, Univ Evry, Université Paris-Saclay, 91025, Evry-Courcouronnes, France*
[2] *LuMIn, CNRS, Institut d'Alembert, ENS Paris-Saclay, Université Paris-Saclay, 91190, Gif-sur-Yvette, France*
[3] *LAMBE, CNRS, CY Cergy Paris Université, 95000, Cergy, France*
[4] *DreamPore S.A.S., 33 Boulevard du Port 95000, Cergy, France*

Received: 31 January 2022 / **Revised:** 11 March 2022 / **Accepted:** 30 March 2022

ABSTRACT

With an increasing global population that is rapidly ageing, our society faces challenges that impact health, environment, and energy demand. With this ageing comes an accumulation of cellular changes that lead to the development of diseases and susceptibility to infections. This impacts not only the health system, but also the global economy. As the population increases, so does the demand for energy and the emission of pollutants, leading to a progressive degradation of our environment. This in turn impacts health through reduced access to arable land, clean water, and breathable air. New monitoring approaches to assist in environmental control and minimize the impact on health are urgently needed, leading to the development of new sensor technologies that are highly sensitive, rapid, and low-cost. Nanopore sensing is a new technology that helps to meet this purpose, with the potential to provide rapid point-of-care medical diagnosis, real-time on-site pollutant monitoring systems to manage environmental health, as well as integrated sensors to increase the efficiency and storage capacity of renewable energy sources. In this review we discuss how the powerful approach of nanopore based single-molecule, or particle, electrical promises to overcome existing and emerging societal challenges, providing new opportunities and tools for personalized medicine, localized environmental monitoring, and improved energy production and storage systems.

KEYWORDS

electric sensor, nanoparticles, environment, biomarkers, energy storage

1 Introduction

The growing global economy and population pose numerous current and future challenges for humanity. Access to affordable health care, environment conservation, and sustainable, abundant, and low-cost sources of energy is some of the key challenges faced by our society. Despite recent slowing in growth rate, the current global population will rise from 7.7 to 9.7 billion people by 2050 [1], further increasing the already high demand for affordable health care, energy, arable land, as well as clean air and water.

Health care provision faces additional challenges due to the increasing average age of the global population. A panoramic view shows a demographic trend for population ageing that is predicted to rise rapidly planetwide. By 2050, the world population aged over 60 will likely reach 2 billion people, compared to 900 million in 2015, a doubling of the population proportion. Today, 125 million people are aged 80 and over, and by 2050, there will be 434 million people in this age group [2]. Ageing impacts health through the increase in chronic diseases, such as diabetes, hypertension, and cancer, but will also lead to an increase of neurodegenerative diseases such as Alzheimer's and Parkinson's. This is compounded by unexpected global events such as the severe acute respiratory syndrome coronavirus-2 (SARS-CoV-2) pandemic that has depressed the global economy through decreased manufacturing, disrupted supply chains, reduced productivity, and overwhelmed health systems [3]. The rapid global spread and severity of illness obliged the entire world to respond quickly to this new challenge. Since 2019, novel coronavirus disease (COVID-19) has been responsible for at least 5.6 million deaths worldwide. The World Bank Group estimates that the global gross domestic product only reached $84 trillion in 2020 and $87 trillion in 2021, a cumulative loss of more than $10 trillion compared to the situation that would have prevailed without the covid pandemic [3]. The total economic cost of this recession could be even higher and difficult to estimate, due to the long-term effects on health, investment, and education. The consequences of such current and future health challenges are significantly increased by the ageing population, which has global impact by affecting general economic productivity, as well as, increasing the need for access to affordable health care.

Emission of pollutants from fossil fuel-based energy production, agriculture, and industry is progressively impacting our environment, with 12.6 million deaths in 2012 estimated to be due to environmental pollutant effects [4]. These emissions also induce global climate changes [5] and natural disasters which affect the entire planet, from soils to oceans, with catastrophic

Address correspondence to Benjamin Cressiot, benjamin.cressiot@cyu.fr; Laurent Bacri, laurent.bacri@univ-evry.fr; Juan Pelta, juan.pelta@univ-evry.fr

consequences for biodiversity, food production, and human population. In addition to well-known pollutants such as greenhouse gasses, pesticides, and other toxic chemicals, nanoparticles have increasingly become a major environmental challenge. In fact, these particles are widely dispersed in the environment. They are detected in the water of rivers or oceans, as is the case for micro- and nano-plastics [6, 7]. After torrential rains, they infiltrate porous soils where they can aggregate with chemical pollutants already present [8, 9]. Soil and waterborne nanoparticles can be absorbed into plant and animal tissues, thus entering the food chain [10, 11]. Nanoparticles are disseminated into the air by emissions from industry or transportation, with transportation emissions also forming carbonaceous particles [12]. They can be produced by agricultural release, natural sources, emission from power generation (fuel or coal), and biomass burning [12]. Nanoparticles are also associated with emissions of chemical compounds such as NH_3 from fertilizer in agriculture, SO_2 and NO_x produced by power generation, and O_3 and NO_x released by land traffic [12]. This complex mixture impacts health through diseases such as asthma, bronchitis, cancer, or cardiovascular disease [12–14]. Nanoparticles are also released from natural events such as sandstorms and forest fires [12, 15] or volcanic eruptions [16, 17], the particles from which can be spread over several continents [14] and are associated with pulmonary disease [18]. However, most of the nanoparticles we encounter are of human origin [12]. They are a component of many common products such as paint, catalytic additives, and cosmetics, and are mostly emitted three ways: 1) during production, 2) during use, and 3) after waste recycling [8]. It is of deep importance to monitor, and understand, how human activities generate these pollutants that impact the environment in order to implement action to reduce these negative effects.

The growing global population and increasing economic development are escalating world energy needs. The global energy rate demand is projected to double from 14 TW (2010) to 28 TW (2050). Using current energy sources, by 2030, this increase will be equivalent to 6.6 million tons of CO_2 produced per hour for every person on the planet [19], leading to an increase in average global temperature of 3 °C by 2100 [5]. To limit global warming below 2 °C, as defined by the global emission challenge, energy production needs to transition to renewable sources to drastically reduce CO_2 emissions. There are different forms of renewable energy to go with the energy transition, for example, solar and biomass energy, geothermal energy, hydropower, and wind power. However, these renewable energies represent only a few % of current global energy consumption, in part due to the unpredictable nature of the weather and tides that power many of these sources [20]. Cost-effective and efficient energy storage methods would counter this unpredictability in supply, however, up to now, the world storage capacity is about 1% of global consumption. The transition towards an ideal zero CO_2 emission in 2050, "climate neutral", or at least a drastic reduction of emission, requires numerous changes in energy generation, use, and storage. These goals include the use of primary energy from renewable energies to recharge the battery storage facilities [21].

Technological advances are providing some solutions to these societal challenges and continued innovation and development of new technology will contribute to management and mitigation of future challenges that arise. As part of this technology-based management, there is a general need to develop monitoring systems that are highly sensitive, *in-situ*, and low-cost, and have single molecule sensing capabilities. Indeed, the lower level of detection sensitivity will allow integration with tightly controlled feedback retroaction, leading to a higher level of safety and efficacy in personalized medicine, environmental control, and energy production, management, and storage.

Nanopore technology provides a solution for these sensing challenges. It is based on a resistive pulse sensing (RPS), where a decrease of the ionic conductance of a nanohole is detected when a single molecule or nanoparticle passes through. This approach based on electrical detection through a nanopore was designed by H. Coulter in 1953 [22]. The electrical detection is optimized in terms of signal to noise ratio when the size of the pore is on the same order as that of the analyte. One of the greatest advantages is the possibility to synthesize different types of nanopores from natural and artificial materials [23–26] targeted to the environmental conditions and the size of the species under study. The electrical signature is sensitive to size, conformation, sequence, chemical nature, and/or charge of the molecule, as well as the nature of ions in the electrolyte solution. Nanopore sensing does not require imaging equipment nor amplification, as in the case of the gold-standard reverse transcription-polymerase chain reaction (RT-PCR). Therefore, it allows the system to scale down to a portable level, like the MinION, developed by Oxford Nanopore Technologies (ONT). Thus, this powerful single molecule technique has great potential to help address the different current and future societal challenges.

In this review, we will focus on nanopore studies that have had, or will have, significant impacts on the fields of health, environment, and energy storage. We first focus on cancer diagnostics through nucleic acid, protein, peptide biomarkers, and virus detection, as well as organic molecule and drug detection. We present approaches to characterize the size and composition of the nanoparticles in the environment disseminated by natural or human activities. We also look at the potential for blue energy and for smart battery diagnosis by nanopore sensing. We conclude this short review with a discussion about the potential perspectives for addressing many of the current and future societal challenges with nanopore technology.

2 Societal health challenges

Since the 90's, there has been a strong effort from the nanopore community to answer biological questions and to address health challenges. Many of these studies were conducted *in vitro*, using biomolecules, and not necessarily connected to direct applications, but were needed from a fundamental aspect to enhance the technology. This review will only focus on concrete results showing how nanopore technology has been applied to health challenges. As presented in Fig. 1, we will discuss a non-exhaustive list of work describing how nanopores can be used for cancer diagnostics and as powerful detectors for protein biomarkers, viral genomes, and particles, as well as organic molecules.

2.1 Cancer diagnostics using nucleic acids

Nanopore technology has been initially focused on nucleic-acid sequencing [35]. While in 1996, the first results were published on DNA transport through an alpha-hemolysin nanopore [36], it was only in 2015 that an Escherichia coli (*E. coli*) genome was assembled *de novo* with 99.5% accuracy using ONT's MinION [37].

Regarding the cancer context, nanopore sequencing has been mainly used to detect structural variants [38, 39] or deletions, inversions, and translocations on tumor suppressor genes in pancreatic cancer [40]. Mutation detection of the TP53 gene has also been explored in patients with chronic lymphocytic leukemia [41, 42]. A wide variety of cancer-related genes such as EGFR, KRAS, NRAS, and NF1 in lung adenocarcinoma have also been sequenced to explain anti-tumor drug sensitivity and resistant mutations [43]. As shown in Fig. 1(1)(a), nanopore technology has been employed to detect and sequence circulating tumor DNA

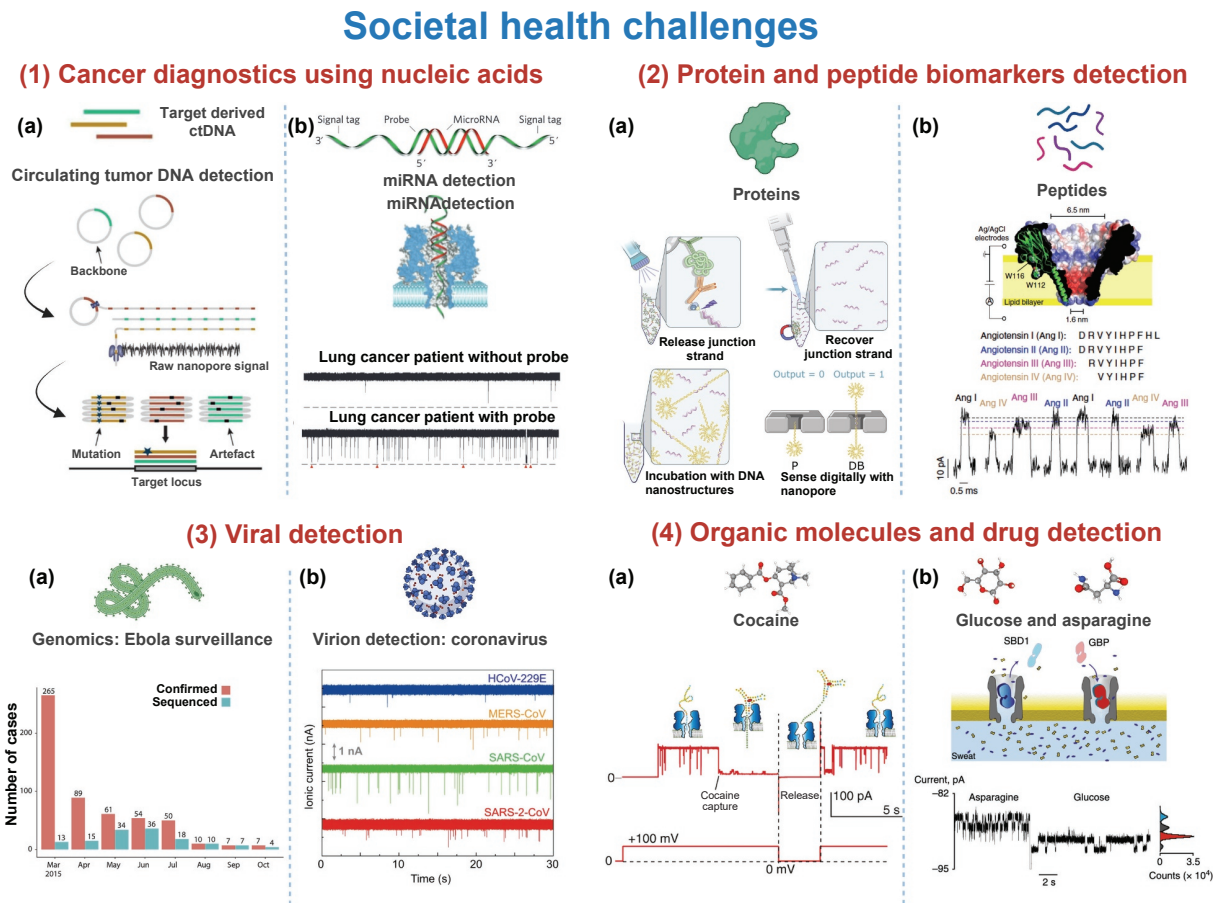

Figure 1 Societal health challenges. (1) Cancer diagnostics using nucleic acids. (a) Circulating tumor DNA detection and CyclomicsSeq protocol. PCR-amplified ctDNA is circularized with an optimized DNA backbone. Rolling circle amplification generates a long DNA molecule with alternating insert and backbone sequences, which is sequenced using ONT's devices. Consensus calling of the DNA sequence allows discrimination between mutations and sequencing artifacts. Reproduced with permission from Ref. [27], © Marcozzi, A. et al. 2021. (b) miRNA detection. miR155 is detected using a probe and an alpha-hemolysin nanopore. Current traces for total plasma RNAs from lung cancer patients without and with the probe. Traces were recorded in 1 M KCl at +100 mV. Red arrows are signature events. Signature events were seen only in the presence of the 100 nM probe. Reproduced with permission from Ref. [28], © Macmillan Publishers Limited 2011. (2) Protein and peptide biomarkers detection. (a) Protein detection. Magnetic beads conjugated with antibodies efficiently capture specific TSH in serum samples and are incubated with secondary antibody conjugated with streptavidin. The immuno-sandwich structure is incubated with biotinylated ssDNA junction strand. The solution is exposed to UV light to release the junction strand. The junction strands are recovered. Shooting star-like DNA probes are added to the solution containing recovered junction strand leading to assembly of a dumbbell-like DNA nanostructure. Digital nanopore sensing to determine the fraction of probes to dumbbells. Reproduced with permission from Ref. [29], © He, L. Q. et al. 2021. (b) Peptide detection. Peptide sequences of angiotensin I (Ang I), angiotensin II (Ang II), angiotensin III (Ang III), angiotensin IV (Ang IV), and typical blockades provoked by the four angiotensin peptides measured at −30 mV through type II W116S-fragaceatoxin C (FraC) nanopores at pH 4.5. Reproduced with permission from Ref. [30], © Huang, G. et al. 2017. (3) Viral detection. (a) Genomics: Ebola surveillance. The number of reported cases of Ebola virus disease in Guinea (red) is shown in relation to the number of EBOV new patient samples (n = 137, in blue) generated during the study. Reproduced with permission from Ref. [31], © Macmillan Publishers Limited 2016. (b) Virion detection: coronavirus. Ionic current time traces showing the detection of cultured HCov-229E, MERS-CoV, SARS-CoV, and SARS-CoV-2 using a solid-state nanopore. Reproduced with permission from Ref. [32], © Taniguchi, M. et al. 2021. (4) Organic molecules and drug detection. (a) Cocaine detection. Typical current–time traces through an alpha-hemolysin nanopore for DNA aptamers with cocaine in 1.0 M KCl, 10 mM PBS, and 1 mM EDTA (pH 7.4). Reproduced with permission from Ref. [33], © American Chemical Society 2011. (b) Glucose and asparagine detection in sweat. Schematic representation and current blockades with their all-point current histogram (below) of two consecutive events showing the entry of SBD1 and GBP into a ClyA nanopore, respectively, under −90 mV applied transmembrane potential in 150 mM NaCl and 15 mM Tris-HCl set to pH 7.5. Reproduced with permission from Ref. [34], © Galenkamp, N. S. et al. 2018. (Created with BioRender.com)

(ctDNA) from a liquid biopsy [27]. This ctDNA harboring the mutations of the original tumor permits the establishment of a molecular diagnosis for cancer monitoring, early-stage detection, and assisting targeted therapy. The authors used a new technique called CyclomicsSeq, where ctDNA is circularized with an optimized backbone. Rolling circle amplification generates a long DNA molecule with alternative insert and backbone sequences. Identifying mutations in the TP53 gene versus assay DNA polymerase induced errors and sequencing artifacts are discriminated by using consensus calling of the DNA sequence.

Nanopores have also been used to detect miRNAs that are short non-coding polynucleotides (an average of 20 nucleotides length). Their differential expression and specific sequences are involved in the initiation and evolution of human cancer [44]. Furthermore, these short miRNAs can be released from a primary tumor into the blood [45]. Figure 1(1)(b) shows that such miRNAs from blood [28] can be detected and identified via a nanopore without amplification using a complementary sequence probe tag for cancer detection. An electrical signature has been observed to detect miR-155 in the plasma of healthy volunteers and patients with lung cancer. The number of events is proportional to the miRNA concentration, which depends on the expression level of this biomarker. The signature frequency for miR-155 hybridized to the probe is higher for patients with lung cancer, and the signal is sensitive up to 0.1 pM. Wanunu et al. showed in another study using a solid-state nanopore [46] that the signal can be sensitive up to 1 fM. Additionally, nanopore technology has demonstrated the ability to detect epigenetic modifications such as CpG

methylation, one of the earliest epigenetic biomarkers for cancer [47–49].

2.2 Protein and peptide biomarkers detection

Protein and peptide detection by nanopore has been extensively studied at a fundamental level. The nanopore community focused their work on understanding the transport dynamics of proteins/peptides through nanopores [50–55], aptamers, and nanopore modifications to control protein capture and selectivity [51, 56–66]. This review focuses only on biomarker detection, the list provided above is not an exhaustive one of what has been published.

Nanopore technology is only recently expanding to protein and peptide biomarkers detection. Biomarkers used for medical analysis are indicators of normal biological and pathogenic processes and are used to assess the risk or presence of disease, pharmacological responses, or course of therapeutic intervention [67]. Up to now, only four publications have shown the potential for these biomarkers [29, 30, 64, 68]. Several recombinant proteins such as endothelin, chymotrypsin, angiotensin, or EGF were detected using an engineered FraC protein nanopore [30].

The other studies used indirect detection methods such as DNA carriers to detect thrombin and acetylcholine from serum using a nanopipette [64]; and to detect prostatic specific antigen bound to DNA aptamers [68] or thyroid stimulating hormone (TSH) with a digital assay [29] using solid-state nanopores (Fig. 1(2)(a)). The presence of TSH is simply detected when two dumbbells linked by a junction are detected through a solid-state nanopore. The authors could quantify TSH from human serum down to the pM range.

Regarding peptide biomarker detection, to the best of our knowledge, there is only one major study showing the potential of nanopore technology to sense peptides with different protein nanopores. Huang et al. used a mutated FraC nanopore with a controllable diameter to discriminate Angiotensin I, II, III, and IV [30] (Fig. 1(2)(b)). The authors showed that they were able to sense each peptide that differed by only a few amino acids. This study is for now the most complete one for peptide biomarker sensing with 17 peptides analyzed. On the other hand, those peptides were not sensed in a complex biofluid.

2.3 Viral detection

The ongoing outbreak of the COVID-19 caused by SARS-CoV-2 has raised a major public health concern worldwide, in which, high-throughput and high-accuracy detection are needed to control these diseases outbreaks. Nanopore sensing generates real-time sequencing data with the potential to become a point-of-care assay. This technique has been already used to identify pathogens, such as chikungunya virus (CHIKV) [69], Ebola virus (EBOV) [31, 69], hepatitis C virus (HCV) [69], human metapneumovirus (HMPV) [70], influenza [71], Lassa fever [72], and SARS-CoV-2 [73] using Oxford Nanopore Technology within a 6–10 h timeframe.

In 2015, researchers used this nanopore technology to provide a real-time genomic surveillance during the EBOV outbreak in West Africa [31]. They provided a robust analysis approach, where it was possible to survey the virus variants (Fig. 1(3)(a)), in which the sequencing process took as little as 15–60 min. This is one of the first steps towards personalized medicine. The individual genetic profile can be used to identify and monitor signatures of viral evolution and drug resistance mutations. This guides the decisions made in regard of diagnosis and characterization of responses to treatments. Moreover, the same system was implemented in the resurgence of the virus last year, providing further insight into the genomic make-up of the viruses [74]. Since polymerase-based assays rely on virus specific primer design that requires prior sequence knowledge, which is unavailable when a new viral outbreak occurs, nanopore sequence technology was crucial in the diagnosis and management of SARS-CoV-2 infections during the first months of the pandemic [75].

The current gold-standard RT-PCR requires highly trained personnel, dedicated facilities, and instrumentations, being time consuming and with limited testing capability. Therefore, to increase test accessibility, other alternatives are necessary. A study using reverse transcription loop-mediated isothermal amplification (RT-LAMP) coupled with a glass nanopore was able to detect SARS-CoV-2 with 98% diagnostic sensitivity and 92% diagnostic specificity [76]. Many publications since SARS-CoV-2 pandemic were published showing the detection of variants by performing complete genome and phylogenetic analysis [73, 77–80]. Bull et al. even describe highly accurate consensus-level sequence determination, with single-nucleotide variants detected at > 99% sensitivity and > 99% precision above a minimum ~ 60-fold coverage depth, thereby ensuring suitability for SARS-CoV-2 genome analysis and confirming the suitability of ONT sequencing for standard phylogenetic analyses.

However, the extraction of viral RNA can be time consuming and presents a risk of exposure to the technician. Solid-state nanopores can have their diameter tuned to match the size of the target nanoparticle providing direct detection of the virus particles. Recently, a method has been reported using a solid-state nanopore in combination with artificial intelligence to detect, *in vitro*, the individual virions from several types of respiratory viruses (Fig. 1(3)(b)) with a discrimination of more than 99% accuracy [32, 81]. Later, this approach was used to detect these viruses in biofluid. In saliva specimens, the authors demonstrated a sensitivity of 90% and specificity of 96% with a 5-min time frame [32]. Furthermore, the use of machine learning technology can be used to discriminate different types of viruses [82, 83], which will enable the development of point-of-care devices with high sensitivity, accuracy, and throughput.

2.4 Organic molecules and drug detection

Since its development in the 90's, nanopore technology has been quickly used to detect drugs and organic molecules. In 1999, the first demonstration of sensing organic molecules was achieved using an alpha-hemolysin modified by a cyclodextrin inserted into its lumen [84]. This cyclic sugar reduced the diameter of the pore so that the authors were able to discriminate between promethazine and imipramine. By modifying alpha-hemolysin, other studies showed the potential for sensing mustard gas analogues [85]. In order to design new or improve existing antibiotics, experiments were conducted to understand how antibiotics can enter bacteria [86]. Several bacterial porins and their mutants were analyzed for a better understanding of antibiotic translocation through these channels and proved to be useful to characterize the physicochemical rules of porin-mediated permeability.

Figure 1(4)(a) shows how Kawano et al. designed a methodology for the rapid and highly selective detection of cocaine using alpha-hemolysin combined with a DNA aptamer [33]. The DNA aptamer recognizes the cocaine molecule with high selectivity. When the aptamer is bound to a cocaine molecule, the complex is trapped inside the nanopore, exhibiting a specific signal. The authors detected a low concentration of cocaine (300 ng·mL^{-1}) within 60 s using this pore embedded in a microchip.

Most of the studies cited above did not detect these molecules from a biofluid. A recent publication showed the potential to directly detect organic molecules such as glucose and asparagine from biofluids (sweat, urine, saliva, and blood) using a protein

nanopore ClyA (Fig. 1(4)(b)) [34]. The system relies on two specific glucose and asparagine protein binders. The proteins having different conformations when bound or unbound to their substrate, the authors were able to sense the conformational state of each binder and quantify indirectly both organic molecules.

3 Societal environmental challenges

Our environment contains a huge diversity of nanoparticles (Fig. 2(1)), which can be discriminated in terms of size (1–1,000 nm), and material, that can be natural materials (e.g., pollen, SiO_2, volcanic ashes, and sulfur gases...), or human made materials (e.g., TiO_2 [87, 88], SiO_2 [89, 90], Ag^+ [9, 88, 91–93], and micro- and nano-plastics [6, 7, 94, 95]).

Nanoparticles produced by human-made materials are unfortunately linked to a market with an estimated size in billions of dollars (TiO_2 $20.9 billion in 2021 [96], SiO_2 $6.45 billion in 2018 [97], and silver $2 billion in 2020 [98]). TiO_2 is used in several industrial fields and enters the composition of paintings, paper, plastic, or cosmetics as a white pigment. These particles are found, for example, in algae [87], or bacteria [88]. SiO_2 is found in nature as quartz, which is one of the most common minerals on earth and is extracted from sand or granite. It is mainly used in architecture and is a compound in concrete for construction. It also plays an important role in the composition of glass or ceramics. Silica nanoparticles are used in chemistry, pharmaceutics, and the food industry. After purification, they are one of the main materials for the high-tech industry of microelectronics or fiber optics. SiO_2 nanoparticles also have cytotoxic properties due to the presence of silanol groups. They can interact with membrane proteins leading to cell damage of the immune system [90]. Their environmental impact has been shown by several publications [89].

Silver nanoparticles are used for their antibacterial properties in biomedicine, and food packaging industry [9, 92]. Toxic effects of small Ag nanoparticles (< 25 nm) could be due to their antibacterial nature and damage to important bacterial biofilms

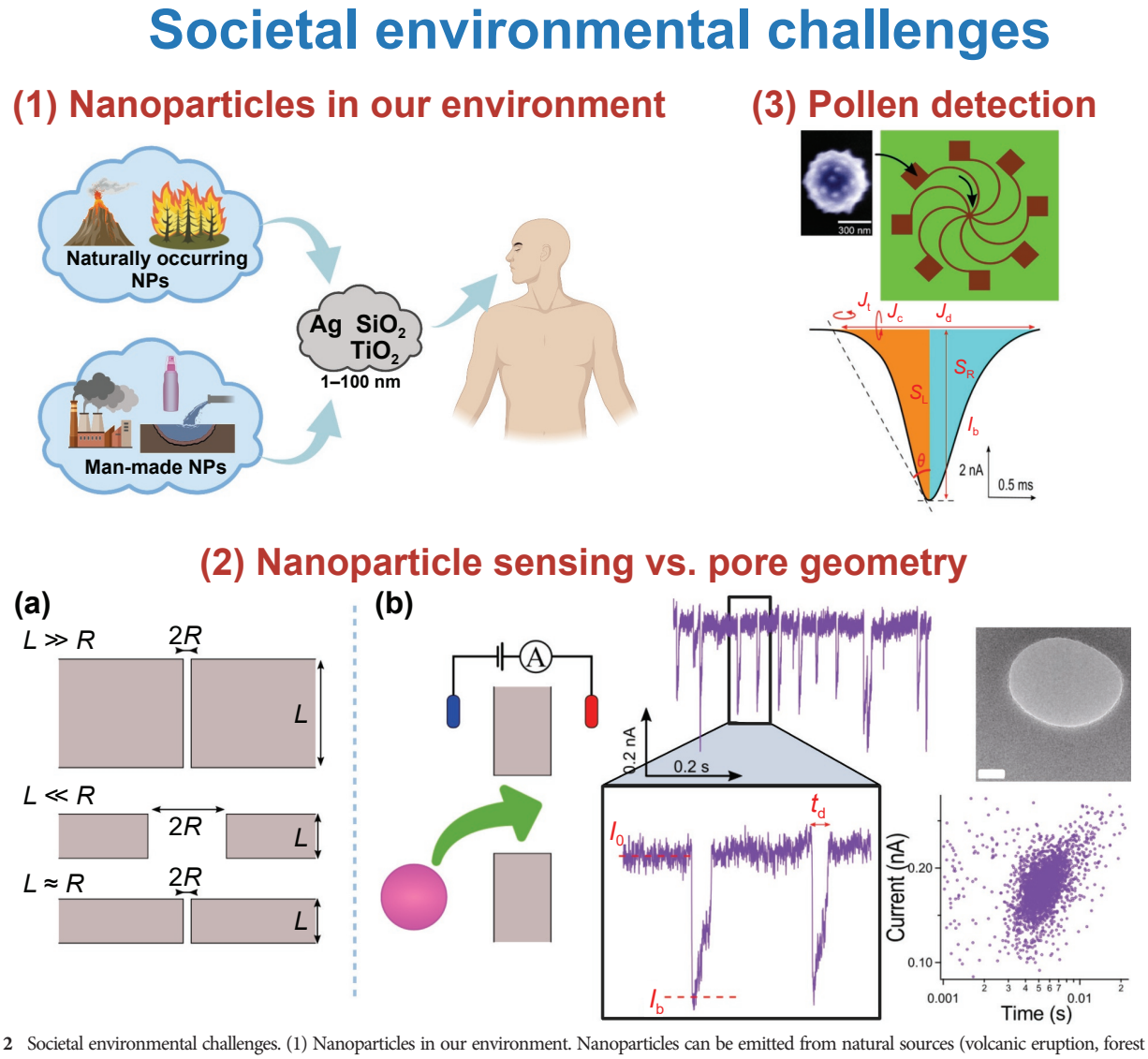

Figure 2 Societal environmental challenges. (1) Nanoparticles in our environment. Nanoparticles can be emitted from natural sources (volcanic eruption, forest fire) or produced by human activities. (2) Nanoparticle sensing vs. pore geometry. (a) Nanopores according to their aspect ratio L/R, where L and R are the length and the radius, respectively. (b) Electrical sensing at the single particle scale. The transport of each nanoparticle through the constriction leads to the transient decrease of the ionic current of the nanopore I_0. Each blockade of 85 nm large SiO_2 nanoparticle is characterized by its duration t_d and its blockade current I_b. Scatter plot of I_b vs. t_d. ΔV = 400 mV, 10 mM KCl. TEM picture of a nanopore. The scale bar is 20 nm long. Reproduced with permission from Ref. [99], © American Chemical Society 2011. (3) Pollen detection. Three-dimensional (3D)-integrated solid-state nanopore for analysis in air. Nanoparticles from cypress pollen (scale bar is 300 nm long) are captured in the spiral-shaped device to be analyzed by the nanopore located in the central area. Current blockade characterized by I_p, t_d, the θ angle, the left area S_L, the right area S_R, and the moment of inertia according to the vertical (J_t) and the horizontal (J_c) axes. Reproduced with permission from Ref. [100], © American Chemical Society 2019. (Created with BioRender.com)

[88, 91]. Moreover, Ag nanoparticles in their cationic form can be dissolved and interact with anions such as citrates to induce crossover toxicity [88, 92, 93].

Nanoparticles in air are analyzed by condensation particle counters (CPC) [101] to measure their concentrations, size distributions, and charges. To discriminate the different shapes, high resolution microscopy is needed such as scanning electron microscopy (SEM) or transmission electron microscopy (TEM) [88, 102]. Atomic force microscopy (AFM) is also able to analyze shapes of nanoparticles or nanofibers [103] or their charge [104]. These devices allow study of the interaction between nanoparticles and lipidic nanotubes [105] and can be supplemented by electrical characterization of lipid bilayer membranes in the presence of nanoparticles [106]. Nanoparticles in solution could be also analyzed by dynamic light scattering (DLS) [88, 107]. However, these sensing methods need to be combined, in order to accurately measure concentration, size, shape, and chemical or charge composition. These methods are expensive and are mainly confined to laboratories, demanding infrastructures, and highly qualified technicians. While still in the early stage of development, we present below a nanopore sensing electrical approach that promises to provide a low-cost, highly sensitive, portable, and real-time monitoring system for nanoparticle pollution.

As described above, RPS is based on electrical detection through a confined constriction playing the role of the sensing head (Fig. 2(2)), which can be optimized for the target nanoparticles. This technology enables both numeric and size analyses of single 90 nm large polystyrene nanoparticles through high aspect-ratio (length L >> radius R) pores in a Nuclepore track-etched membrane [108]. Recently, Balme et al. have designed single track-etched pores to detect 40–100 nm large polystyrene nanoparticles [109]. In 2004, Ito et al. have shown a single long carbon nanotube was able to both analyze size and surface charge of functionalized polystyrene particles [110].

Electron beam lithography has enabled the fabrication of very low aspect-ratio (L << R) 100 nm–1 μm sized pores in 50 nm –1 μm thick membranes of Si [111, 112] or SiN_x membranes [100, 113] for the detection of 50–800 nm large polystyrene or gold nanoparticles.

The medium aspect-ratio pores ($L \approx R$) are obtained by drilling 20–100 nm thin membranes. The material used to make these membranes is mainly SiN_x, but SiO_2 can also be used for the analysis of carboxylate modified 100–200 nm nanobeads [114] or 11 nm × 68 nm gold nanorods [115]. Promising materials such as hafnium oxide for 10 nm gold nanoparticle sensing [115] or titanium nitride, titanium-tantalum and tantalum have also been used to detect 100 nm polystyrene nanoparticles coated with DNA [116].

The largest nanopores (135–300 nm) are drilled in 50–500 nm thick membranes by focused ion beam (FIB) milling for the detection of single particles on the scale of silicate [99, 117], latex [118, 119], gold [120], and polystyrene [121, 122] nanoparticles. Smaller nanopores below 40 nm are drilled by an electron beam issued from a TEM to optimize the sensing of nanoparticles below 10 nm [115, 123].

The statistical analysis of current blockade experiments is mainly based on the blockade rate, duration, or amplitude. The blockade rate allows the nanoparticle concentration to be estimated according to the amplitude of the energy barrier that must be crossed to enter the nanopore [99, 116]. The amplitude is a function of the nanoparticle size or shape [99, 108, 110, 123]. The duration makes it possible to describe the transport dynamics through the nanopore [99]. As the transport is mainly controlled by a difference of applied potential, the charge [99, 112, 123] or the electrophoretic mobility [110] can also be evaluated. In the case of neutral nanoparticles, the flow rate is governed by a difference of applied pressure such as hydrostatic [118, 124] or osmotic pressure [30].

A recent publication has shown an interesting microfluidic device to capture nanoparticles disseminated in air (Fig. 2(3)). This method allows discrimination between cedar and cypress pollens from their current blockades and duration distributions [100]. Machine learning algorithms can be used to determine which pair of parameters is relevant to identify the different pollen types and can be generalized to the detection of other particles [62, 125].

In all cases, a microfluidic architecture to be combined with the nanopore detector is crucial in theses monitoring systems, not only to manage the fluid handling and delivery to the nanopore, using specific surface functionalization [56, 57], but also to include pre-filtering functions or fluid addressing functions for high throughput approaches [126], or even to stabilize the nanopore and its lipid bilayer microenvironment in case of biological nanopores [127].

4 Societal energy challenges

4.1 Blue energy

The fast growth of global energy consumption and the need to limit the effects of global climate change through transition from fossil fuel-based energy production require new energy sources. Renewable energy plays an important role in reducing greenhouse gas emissions, associated with global warming. It allows the conservation of natural resources, lowers carbon emission, and avoids contamination of air and water. As the name suggests, it is created from natural sources such as sunlight [128], wind [129, 130], biomass [131], geothermal [132], and water salinity gradients [133–137]. The latter, also known as blue energy, present a promising energy source if we consider the availability of energy coming from the osmotic pressure difference between seawater and fresh water or wastewater [136]. The two most promising methods to harness the salinity gradient energy are i) pressure-retarded osmosis (PRO) [138, 139], a water flow through semipermeable membranes (Fig. 3(1)(a)), and ii) reverse electrodialysis (RED) [140–142], which uses ion-exchange membranes (IEMs) (Fig. 3(1)(b)). The main difference between them relies on the molecule being transported through the semiporous membrane that is composed by an array of nanopores, water, or ions, respectively. Up to now, their major limitations are their low energy efficiency, and the cost and fouling of membranes [137, 143, 144]. The semipermeable membranes do not have an adequate water flow [145]. The membrane support present an internal concentration polarization, which considerably reduces permeate-water flux, thus reducing the power density. A pilot plant in Norway could generate less than 1 $W \cdot m^{-2}$ using commercial, asymmetrical cellulose-acetate membranes [145]. Thus, the development of new materials and techniques are fundamental. Recently, ion-selective nanochannels have been exhibiting promising results to harvest blue energy (Fig. 3(1)(c)) [146, 147].

Siria et al. showed that boron nitride nanotubes (BNNTs) present an enhancement of the osmotic current, reaching a power density about 4 $kW \cdot m^{-2}$ for a single BNNT using a RED configuration (Fig. 3(2)(a)) [148]. Later on, a two-dimensional (2D) single-layer molybdenum disulfide (MoS_2) nanopore reached a power density about 1 $MW \cdot m^{-2}$ in alkaline solution [149]. These studies report an increase in the magnitudes of energy generated. Recently, nanoporous carbon membranes made from core–rim polycyclic aromatic hydrocarbons reached a maximum value of

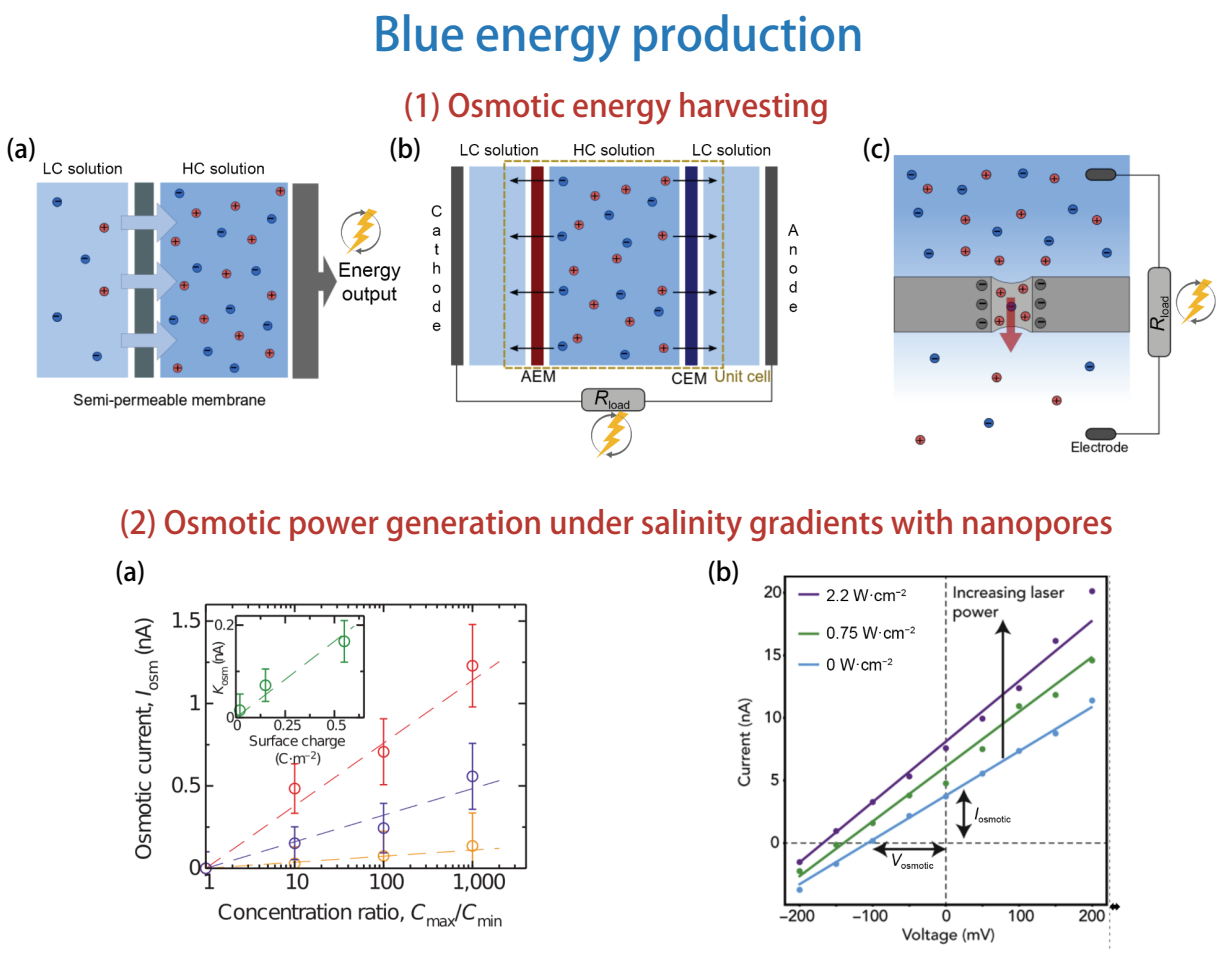

Figure 3 Blue energy production. (1) Osmotic energy harvesting. (a) Schematic of PRO configuration. In PRO, the high-concentration (HC) draw solution and the low-concentration (LC) feed solution are separated by a semi-permeable membrane. At ideal conditions, only water molecules move from low to high concentration. As water flows into the HC chamber, the pressurized solution propels a hydro turbine to generate energy. (b) Schematic of RED configuration. In RED, the energy is generated by the concentration difference across IEMs, in which, cation-exchange membranes (CEMs) and anion-exchange membranes (AEMs) are stacked alternately between the low and high concentration solutions. The ion flux, positive ions moving one way and the negative ones moving in the counter direction, creates an electrochemical difference that is converted into an electrical current at the electrodes and a work is produced by the load resistor, generating energy. (c) Schematic of harvesting osmotic energy with a negative charged solid-state nanopore. Electrolytes with different salt concentration are separated by a nanopore membrane. A mostly positive charged ion flux is driven by the chemical potential through the negatively charged nanopore. (2) Osmotic power generation under salinity gradients with nanopores. (a) Osmotic streaming current versus concentration difference for a transmembrane boron nitride nanotube (t-BNNT) with {*R*, *L*} = {40 nm, 1,250 nm} and pH 5.5 (yellow), 9.5 (purple), and 11 (red). The experimental points show measurements for various salt concentrations (*C*) in the two reservoirs, with C_{min} and C_{max} in the range 10^{-3}–1 M. Error bars follow from the corresponding error analysis. Dashed lines are linear fits for measured osmotic current: $I_{osm} = K_{osm}\log(C_{max}/C_{min})$. Inset, osmotic mobility (K_{osm}) versus surface charge. Surface charge is obtained from independent conductance measurements. The dashed line is a linear fit: $K_{osm} \approx 0.33\Sigma$, where Σ is the surface charge density on the BNNT surface. Reproduced with permission from Ref. [148], © Macmillan Publishers Limited 2013. (b) Current vs. voltage (*I*–*V*) characteristics at a concentration gradient of 1:1,000 using different laser intensities. Reproduced with permission from Ref. [147], © Elsevier Inc. 2019. (Created with BioRender.com)

67 W·m^{-2} with a cationic selectivity [150]. The technique used paves a way to large-scale fabrication of nanopores arrays with a small pore size distribution and a good ionic selectivity.

Changes in the nanochannel size and shape can also optimize its performance. A study comparing different types of nanochannels: bullet-shaped, conical, and trumpet-shaped nanochannels, reported that trumpet-shaped nanochannels presents the best ion selectivity while the bullet-shaped one presents a local maximum of power harvesting [133]. As cited before, MoS_2 monolayer membranes provided one of the best efficiencies in producing energy. By increasing their surface charge with light irradiation, it is possible to double the osmotic power generated using a single nanopore at neutral pH (Fig. 3(2)(b)) [147].

4.2 Sensing battery with nanopores

Batteries, as one of the most versatile energy storage technologies, play a central role in the ongoing transition from fossil fuels to renewable energy [19]. They have become key enablers for the deployment of electric transportation and the use of decentralized renewable energy sources. With batteries becoming the heart of future society, generation of smart batteries should support this change in the energy economy and is a fundamental element of sustainable development [151, 152]. A key feature of such battery design is the incorporation of smart functionalities, for example, sensing and diagnosis [153], self-healing and recovery [154] to increase the initial lifespan, to allow reconditioning for reuse, to develop and manufacture more eco-compatible battery, and to recycle battery elements as much as possible. Indeed, there is a crucial need to improve their quality, reliability, and life by non-invasive *in operando* performance monitoring and control of their state of health, state of charge, state of energy, state of power, and state of safety [153].

The principle of a rechargeable battery is an electrochemical cell composed of a cathode and an anode, positive and negative electrodes respectively, separated by an ion-containing electrolyte

solution. Electrodes are connected to an electrical circuit that allows the electron flow, while the ion flow is only possible through the electrolyte. Simultaneous electrochemical reactions occur at the two electrodes, leading to the charge (energy storage) and the discharge of the battery (energy delivery), depending on the electron flow direction [155] (Fig. 4(1)).

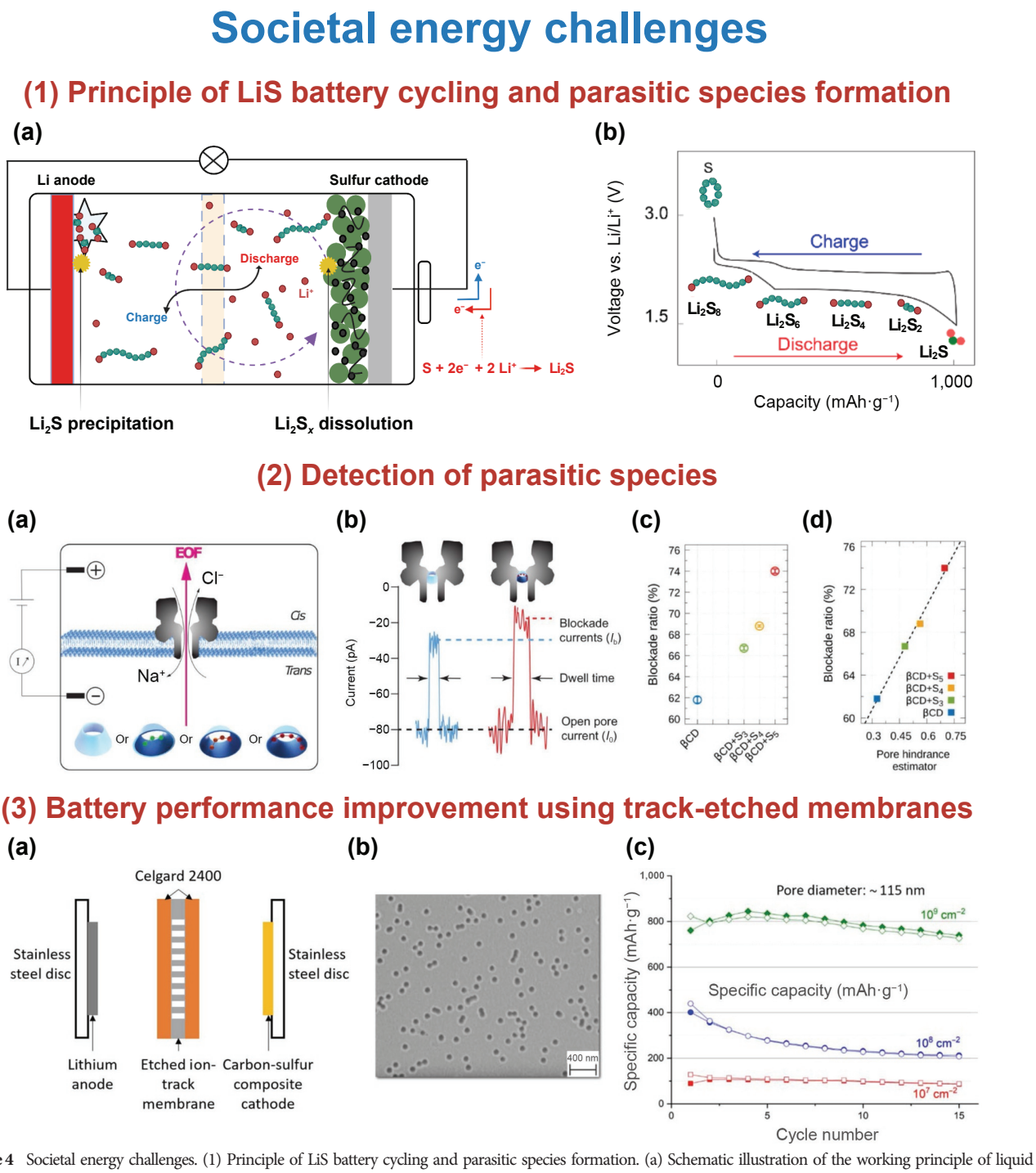

Figure 4 Societal energy challenges. (1) Principle of LiS battery cycling and parasitic species formation. (a) Schematic illustration of the working principle of liquid electrolyte Li-S battery exhibiting the parasitic polysulfide red-ox shuttle. (b) First galvanostatic discharge and charge voltage profiles enlightening the stepwise cathodic reduction of S involving the formation of the intermediate polysulfides originating from the two plateaus. (2) Detection of parasitic species using a protein nanopore. (a) Schematic of the ion–current measurement set-up. One protein nanopore is inserted into a suspended lipid bilayer. An electrical potential is applied via two Ag/AgCl electrodes, which induces an ionic current of Na^+ and Cl^- ions through the nanopore (1 M NaCl, 25 mM $NaHCO_3$, pH 10, under argon atmosphere). At pH 10, the α-HL is anion selective, consequently, an EOF directed from trans to cis sets in favoring the entry of β-cyclodextrin and Na_2S_x/β-cyclodextrin into the stem part of the α-HL. (b) Detail of a part of current trace blockades arising from β-cyclodextrin (blue) and from Na_2S_5/β-cyclodextrin complex (red) interaction with the pore at −100 mV. I_0 is the ionic open pore current and I_b the blockade current. (c) Experimental current blockades. Error bars are the confidence intervals of the average estimator. (d) Nanopore hindrance estimator calculated from atomistic model. Reproduced with permission from Ref. [166], © Bétermier, F. et al. 2020. (3) Battery performance improvement using track-etched membranes. (a) Expanded view of the different components in the coin cell. The separator configuration between the Li anode and the carbon-sulfur cathode consists of the track-etched PET membrane sandwiched between two SK Innovation membranes soaked with electrolyte. (b) Surface view of PET etched ion-track membrane with average pore diameter ~ 100 nm and pore density of 2.5 cm^{-1} × 109 cm^{-1} (~ 25 pores per μm^2). (c) Cycling performance of Li-S coin cells with PET etched ion-track membrane sandwiched between two SK innovation separators for fixed pore diameter of ~ 115 nm and various pore densities. Charge (solid symbols) and discharge (empty symbols) capacities. Reproduced with permission from Ref. [172], © Lee, P. L. J. et al. 2021. (Created with BioRender.com)

One of the challenges in the energy storage field using batteries is the ability to sense, with high specificity and high sensitivity, the health state of a battery for diagnostic analysis either during cycling or post-mortal analysis [153]. The next step will be to cure battery degradation by self-healing functions [154]. Moreover, self-healing is a natural evolutionary process of living organisms, to repair diverse types of damage to increase their lifetime. The kinetics of this process is between minutes to months, respectively for blood coagulation and bone fissure or fracture repair. The performance and lifetime of many rechargeable batteries are limited by two main problems, (I) mechanical degradation: electrode cracking, silicon anode degradation, electrical contact loss, and chemical and (II) electrochemical degradation: electrolyte degradation/formation of solid electrolyte interphase (SEI), lithium plating/dendrite formation, gas evolution, metal dissolution, and degradation of inactive components (binders, separators, and current collectors). Several approaches are being developed to limit battery degradation, for example, self-healing binders, polymers, electrolytes, artificial SEI, the use of microcapsules for the vectorization and the deliverance of conductive additives, and the design of smart separators [154].

We discuss now the ability, in the future, to apply nanopore technology to Li-ion battery diagnostics in order to prevent their degradation and to improve their performance. For energy storage and conversion, the conception of new electrochemical devices compatible with sustainable development has become essential. Indeed, there is a need to develop electrode materials with potential higher capacity and based on abundant materials. This has motivated concerted research efforts towards new systems beyond Li-ion, for instance the Li-sulfur battery with five times more theoretical specific energy ($Wh{\cdot}kg^{-1}$), significantly improving the size/weight to energy capacity ratio, an important consideration in electric transportation [156]. Although quite appealing, this system suffers from poor performances associated with difficulties in mastering–limiting the polysulfide (polyS) redox shuttle process [157]. Redox shuttles are also responsible for part of the capacity decay observed in today's Li-ion batteries. This capacity loss is due to polysulfide solubility (S_8^{2-}, S_6^{2-}, etc.) in the electrolyte. These chemical species result from reduction of sulfur by lithium. This step is necessary to get the fully reduced and insoluble Li_2S. Polysulfide can then diffuse to the Li^0 electrode, be reduced there, and passivate the surface of the negative electrode. This process consumes sulfur, the active material of the positive electrode. Furthermore, the longest polysulfide chains can be only partially reduced on the Li^0 surface and diffuse back to the positive electrode where they can be oxidized again. Such a back-and-forth process is known as redox shuttle.

Interesting analytical techniques already exist to identify redox species and monitor, for instance, Li-S batteries electrolyte composition [158] such as ultraviolet–visible (UV–vis) spectra [159], differential cyclic voltammetry [160], nuclear magnetic resonance (NMR) [161], X-ray [162], mass spectrometry [163], fiber Bragg grating sensors [164], or tilted sensors [165]. These techniques are useful, but expensive, and some of them require infrastructure and operational expertise. The bulk approach does not allow detection of the size, sequence, or chemical reaction, at the single molecule level, of these parasitic redox species at the beginning of their formation.

Recently the proof-of-concept has been shown, in aqueous medium, to identify polyS species with a protein nanopore and using a cyclodextrin (CD) adaptor [166]. Na-based polysulfide species Na_2S_n (n = 3, 4, and 5) in aqueous media can be found as catholyte in aqueous Na-ion/polysulfide batteries [157]. The best affinities for β-CD-polysulfides complexes are found in comparison to alpha and gamma-CD, the interaction is reversible by temperature. Only one molecule of polyS is inside the cavity of the CD. The affinity increases with the polysulfide length in the complexation. The CD alone or the complex enters toward the stem side of alpha-hemolysin by the electro-osmotic flux (EOF) driving force contribution (Fig. 4(2)(a)). The blockade ratios from the current traces show a specific signature for each species of polysulfide (see Fig. 4(2)(b)). This signature is mainly due to the steric volume of the complex inside the nanopore (Fig. 4(2)(c)). A good correlation is obtained between the blockage ratio and the pore hindrance estimator. Finally, this work demonstrated polysulfide detection and discrimination, with single sulfur resolution, in aqueous medium using a protein nanopore.

One of the next challenges in the future is to implement the nanopore approach in battery conditions. Up to now, it is impossible to work with a biological membrane and nanopore, mainly composed of lipids, in organic solvent. Several options are possible, such as the use of a polymer membrane [167, 168] or a solid-state membrane [26] to design a hybrid nanopore [169–171]. Protein channels are hardly used in non-aqueous mediums. It is therefore necessary to find or to design new class of highly stable protein nanopores.

Different polymers can be used to manufacture track-etched membranes in order to make them resistant to multiple solvent conditions [168]. It is possible to control the pore density in the membrane from a single nanopore up to 10^{10} $pore{\cdot}cm^{-2}$, the pore diameter nanometric to micrometric and also the thickness of the membrane ranging from 6 to 50 μm [168]. Recently, polyethylene terephthalate (PET) membranes containing nanopores have been designed and used as a separator for Li-S coin cells battery to increase their performance [172]. The PET separator is sandwiched between two Celgard 2400 membranes soaked with electrolyte. The separator is inserted between the Li anode and the carbon-sulfur cathode (Fig. 4(3)). By cycling only 15 times, the Coulombic efficiency is maintained of up to 97% with minor reduction in capacity as a function of nanopore diameter and density used.

5 Conclusion and perspectives

We observe that most of the attention from the nanopore community had been focused on societal health challenges. Due to devices and application protocols from Oxford Nanopore Technologies, rapid nucleic-acid sequencing by nanopores has become routine. We saw that researchers adapt the sequencing system for better accuracy or specific identification of mutations in genes implicated in cancer. The portable MinION sequencer offers the prospect of personalized medicine, such as the example given with Ebola surveillance [31, 74] or recently seen in SARS-CoV-2 diagnosis and genome analysis [75, 173]. The nanopore technique is extremely powerful in detecting organic molecules and shows promising results in searching for biomarkers in infinitesimal (high femtomolar range) [29] quantities from biofluids [34]. On the other hand, the technique could still lack sensitivity and selectivity to directly detect a biomarker in a complex fluid without microfluidic pre-filtering or a molecular carrier.

Regarding proteins, only a tiny percent of the human genomic DNA encodes for them. Additionally, protein isoforms, variants, and chemical modifications are not coded in the genome either. The resulting protein diversity is deeply involved in normal and diseased cellular processes. We are at the start in detecting proteins and peptides as biomarkers and in a race to design protein sequencers by nanopores [174, 175]. Cellular protein information, often used as a source of biomarkers, is of great importance for early disease detection. Recent publications showed that actual nanopores are sensitive enough to identify amino acid

composition [30, 176–179] and posttranslational modifications [180–183], opening a new era in proteomics. Researchers are also exploring protein fingerprinting [184]. The idea relies on measuring peptide spectra produced from hydrolyzed proteins, such as seen in mass spectrometry, allowing their identification. A recent publication also showed that a DNA-peptide conjugate could be pulled through a protein nanopore MspA by a DNA helicase Hel308 allowing multiple rereads in the ionic current signal enabling discrimination of single-amino acid substitutions in single reads [185–187]. This proof-of-concept opens excellent prospects for sequencing proteins and peptides.

One of the societal issues in health that has not been addressed in this review is understanding the processes of protein aggregation in neurodegenerative diseases such as Alzheimer's disease and how to prevent this pathological aggregation. Some studies have been able to follow this dynamic of aggregation *in vitro* by nanopore with recombinant proteins, mainly using artificial, track-etched, and glass nanopores [51, 188–190]. On the other hand, no study has been conducted using biological material from patients to date.

The nanoparticles released into the environment are disseminated in the air, soil, and water. Eventually, we find them in the food we eat or in the air we breathe. Several analytical techniques must be combined in a laboratory with highly qualified people to characterize the concentrations, sizes, shapes, or composition of each nanoparticle. Based on electrical sensing at the nanoparticle level, the RPS approach can meet this challenge as it was the case for nano-plastic or silicate nanoparticle. Nevertheless, this technique should be extended to TiO_2 and silver nanoparticles to follow environment pollution. Until now, these RPS devices remain confined to the laboratory. In the future, they will be used, *in situ*, near the source of pollution in the air or along the river by taking the design of portable devices into account. As these sensors require low energy, they could be inserted in autonomous devices to monitor environments in real time when connected to a wireless network.

A similar approach based on the confined transport of ions will be used to produce renewable, clean, and non-intermittent source of energy, to answer the increase in energy consumption caused by economic and population growth, if we want to preserve the planet for future generations. The energy conversion coming from salinity gradients, also known as blue energy, has been explored as a promising immense and untapped source of energy. However, the large-scale implementation of PRO and RED system has been hindered by the low efficiency of the current harvesting technology, mainly due to the low power density at scales beyond the ones produced in laboratories. Advances in the material science and nanofluidic transport reported findings of extremely high osmotic power densities, which could further be increased using nanopore arrays along the membrane or using natural sources (e.g., sunlight) to generate charges along the membrane surface to optimize power generation.

Beyond developing new ways to produce energy, there is a need to increase storage capability of the current batteries. Nanopore technology also offers solutions to this challenge. The approach to health diagnostics and personalized medicine could continue to inspire the field of energy storage with a new generation of batteries that must conform to sustainable development. Thus, it would be necessary to be able both to perform a diagnosis of the state of health of a battery and to be able to repair *in situ* the degradation. To heal batteries, it will be necessary to add repair functions integrated into the battery that are activatable according to a stimuli related to a threshold of battery degeneration.

Considerable work remains to be done for the detection and characterization of parasitic species in batteries and to probe the chemical reactions associated with the formation of these species, even if the proof-of-concept has just been shown, in an aqueous environment, on the ability of a nanopore to identify parasitic species, polysulfides, with a discrimination resolution of a single sulfur and the ability to complex them with cyclodextrins [166]. It will be a huge challenge, for several reasons, to design and synthesize the required materials to manufacture the nanopores according to the specifications of the harsh battery environment. In addition, there is work remaining to integrate such an electrical sensor into a battery. Another, less complex approach would be to proceed by taking samples during the operating cycles of the battery life, but also for post-mortem analysis.

The coupling between electrical detection with nanopore sensor and damage repair is also a perspective to be developed in the upcoming years. It will be interesting to manufacture smart separators that could early detect and identify parasitic species to capture them effectively. In particular, the functionalization of polymeric membranes could provide a solution.

In this review, we discuss how the nanopore technique, based on single-molecule, or particle, electrical sensing affords methods to address many of the existing and emerging societal challenges in health care, environmental monitoring, and energy provision or storage. Indeed, the success of nanopore genome sequencing as a tool to manage health, including the SARS-CoV-2 pandemic, one of the greatest health challenges faced by humanity in the last century, is proof of the potential power of nanopore electrical sensors as solutions for emerging and future societal challenges. This technology will provide tools for the development of highly sensitive, real-time, integrated, or on-site sensing to monitor personal health, environmental emissions, and battery health in new smart battery designs. This technology has great potential in applications such as blue energy harvesting and self-healing smart batteries to provide reliable sources of renewable energy for the growing global economy and population. In summary, nanopore technology, along with other innovations, will contribute to the global maintenance of affordable healthcare, clean air and water, arable land, and cheap renewable energy.

Acknowledgements

We acknowledge financial support from DIM Respore, Region Ile de France (PhD grants), ANR Epsilomics (No. 17-CE09-0044-02), CY Initiative of Excellence ("Investissements d'Avenir" No. ANR-16-IDEX-0008), and Réseau sur le Stockage Electrochimique de l'Energie (RS2E).

References

[1] United Nations. *Population* [Online]. United Nations: New York. https://www.un.org/en/global-issues/population (accessed Jan 29, 2022).

[2] Ageing and Health. https://www.who.int/news-room/fact-sheets/detail/ageing-and-health (accessed Jan 25, 2022).

[3] The World Bank. *The World Bank Group's Response to the COVID-19 (Coronavirus) Pandemic* [Online]. The World Bank Group: Washington. https://www.worldbank.org/en/who-we-are/news/coronavirus-covid19 (accessed Jan 25, 2022).

[4] Healthy Environment, Healthy People | UNEP-UN Environment Programme. https://www.unep.org/resources/publication/healthy-environment-healthy-people (accessed Feb 28, 2022).

[5] Making Peace With Nature | UNEP-UN Environment Programme. https://www.unep.org/resources/making-peace-nature (accessed Jan 29, 2022).

[6] Alimi, O. S.; Budarz, J. F.; Hernandez, L. M.; Tufenkji, N. Microplastics and nanoplastics in aquatic environments: Aggregation, deposition, and enhanced contaminant transport.

Environ. Sci. Technol. **2018**, *52*, 1704–1724.
[7] Bouwmeester, H.; Hollman, P. C. H.; Peters, R. J. B. Potential health impact of environmentally released micro- and nanoplastics in the human food production chain: Experiences from nanotoxicology. *Environ. Sci. Technol.* **2015**, *49*, 8932–8947.
[8] Bundschuh, M.; Filser, J.; Lüderwald, S.; McKee, M. S.; Metreveli, G.; Schaumann, G. E.; Schulz, R.; Wagner, S. Nanoparticles in the environment: Where do we come from, where do we go to. *Environ. Sci. Eur.* **2018**, *30*, 6.
[9] Tortella, G. R.; Rubilar, O.; Durán, N.; Diez, M. C.; Martínez, M.; Parada, J.; Seabra, A. B. Silver nanoparticles: Toxicity in model organisms as an overview of its hazard for human health and the environment. *J. Hazard. Mater.* **2020**, *390*, 121974.
[10] Lu, Y. F.; Zhang, Y.; Deng, Y. F.; Jiang, W.; Zhao, Y. P.; Geng, J. J.; Ding, L. L.; Ren, H. Q. Uptake and accumulation of polystyrene microplastics in zebrafish (*Danio rerio*) and toxic effects in liver. *Environ. Sci. Technol.* **2016**, *50*, 4054–4060.
[11] Sun, X. D. ; Yuan, X. Z. ; Jia, Y. B. ; Feng, L. J. ; Zhu, F. P. ; Dong, S. S. ; Liu, J. J. ; Kong, X. P. ; Tian, H. Y. ; Duan, J. L. et al. Differentially charged nanoplastics demonstrate distinct accumulation in *Arabidopsis thaliana*. *Nat. Nanotechnol.* **2020**, *15*, 755–760.
[12] Lelieveld, J.; Evans, J. S.; Fnais, M.; Giannadaki, D.; Pozzer, A. The contribution of outdoor air pollution sources to premature mortality on a global scale. *Nature* **2015**, *525*, 367–371.
[13] Czarny, B.; Georgin, D.; Berthon, F.; Plastow, G.; Pinault, M.; Patriarche, G.; Thuleau, A.; L'Hermite, M. M.; Taran, F.; Dive, V. Carbon nanotube translocation to distant organs after pulmonary exposure: Insights from *in situ* ^{14}C-radiolabeling and tissue radioimaging. *ACS Nano* **2014**, *8*, 5715–5724.
[14] Buzea, C.; Pacheco, I. I.; Robbie, K. Nanomaterials and nanoparticles: Sources and toxicity. *Biointerphases* **2007**, *2*, MR17–MR71.
[15] Reid, C. E.; Brauer, M.; Johnston, F. H.; Jerrett, M.; Balmes, J. R.; Elliott, C. T. Critical review of health impacts of wildfire smoke exposure. *Environ. Health Perspect.* **2016**, *124*, 1334–1343.
[16] Ermolin, M. S.; Fedotov, P. S.; Malik, N. A.; Karandashev, V. K. Nanoparticles of volcanic ash as a carrier for toxic elements on the global scale. *Chemosphere* **2018**, *200*, 16–22.
[17] Trejos, E. M.; Silva, L. F. O.; Hower, J. C.; Flores, E. M. M.; González, C. M.; Pachón, J. E.; Aristizábal, B. H. Volcanic emissions and atmospheric pollution: A study of nanoparticles. *Geosci. Front.* **2021**, *12*, 746–755.
[18] Jeevanandam, J.; Barhoum, A.; Chan, Y. S.; Dufresne, A.; Danquah, M. K. Review on nanoparticles and nanostructured materials: History, sources, toxicity and regulations. *Beilstein J. Nanotechnol.* **2018**, *9*, 1050–1074.
[19] Larcher, D.; Tarascon, J. M. Towards greener and more sustainable batteries for electrical energy storage. *Nat. Chem.* **2015**, *7*, 19–29.
[20] Lewis, N. S. Powering the planet. *MRS Bull.* **2007**, *32*, 808–820.
[21] Tarascon, J. M. Les batteries sont-elles la bonne option pour un développement durable. *C. R. Geosci.* **2020**, *352*, 401–414.
[22] Coulter, W. H. Means for counting particles suspended in a fluid. U. S. Patent 2, 656, 508, October 20, 1953.
[23] Shi, W. Q.; Friedman, A. K.; Baker, L. A. Nanopore sensing. *Anal. Chem.* **2017**, *89*, 157–188.
[24] Cressiot, B.; Ouldali, H.; Pastoriza-Gallego, M.; Bacri, L.; van der Goot, F. G.; Pelta, J. Aerolysin, a powerful protein sensor for fundamental studies and development of upcoming applications. *ACS Sens.* **2019**, *4*, 530–548.
[25] Lepoitevin, M.; Ma, T. J.; Bechelany, M.; Janot, J. M.; Balme, S. Functionalization of single solid state nanopores to mimic biological ion channels: A review. *Adv. Colloid Interface Sci.* **2017**, *250*, 195–213.
[26] Xue, L.; Yamazaki, H.; Ren, R.; Wanunu, M.; Ivanov, A. P.; Edel, J. B. Solid-state nanopore sensors. *Nat. Rev. Mater.* **2020**, *5*, 931–951.
[27] Marcozzi, A.; Jager, M.; Elferink, M.; Straver, R.; van Ginkel, J. H.; Peltenburg, B.; Chen, L. T.; Renkens, I.; van Kuik, J.; Terhaard, C. et al. Accurate detection of circulating tumor DNA using nanopore consensus sequencing. *npj Genom. Med.* **2021**, *6*, 106.
[28] Wang, Y.; Zheng, D. L.; Tan, Q. L.; Wang, M. X.; Gu, L. Q. Nanopore-based detection of circulating micrornas in lung cancer patients. *Nat. Nanotechnol.* **2011**, *6*, 668–674.
[29] He, L. Q.; Tessier, D. R.; Briggs, K.; Tsangaris, M.; Charron, M.; McConnell, E. M.; Lomovtsev, D.; Tabard-Cossa, V. Digital immunoassay for biomarker concentration quantification using solid-state nanopores. *Nat. Commun.* **2021**, *12*, 5348.
[30] Huang, G.; Willems, K.; Soskine, M.; Wloka, C.; Maglia, G. Electro-osmotic capture and ionic discrimination of peptide and protein biomarkers with FraC nanopores. *Nat. Commun.* **2017**, *8*, 935.
[31] Quick, J.; Loman, N. J.; Duraffour, S.; Simpson, J. T.; Severi, E.; Cowley, L.; Bore, J. A.; Koundouno, R.; Dudas, G.; Mikhail, A. et al. Real-time, portable genome sequencing for Ebola surveillance. *Nature* **2016**, *530*, 228–232.
[32] Taniguchi, M.; Minami, S.; Ono, C.; Hamajima, R.; Morimura, A.; Hamaguchi, S.; Akeda, Y.; Kanai, Y.; Kobayashi, T.; Kamitani, W. et al. Combining machine learning and nanopore construction creates an artificial intelligence nanopore for coronavirus detection. *Nat. Commun.* **2021**, *12*, 3726.
[33] Kawano, R.; Osaki, T.; Sasaki, H.; Takinoue, M.; Yoshizawa, S.; Takeuchi, S. Rapid detection of a cocaine-binding aptamer using biological nanopores on a chip. *J. Am. Chem. Soc.* **2011**, *133*, 8474–8477.
[34] Galenkamp, N. S.; Soskine, M.; Hermans, J.; Wloka, C.; Maglia, G. Direct electrical quantification of glucose and asparagine from bodily fluids using nanopores. *Nat. Commun.* **2018**, *9*, 4085.
[35] Deamer, D.; Akeson, M.; Branton, D. Three decades of nanopore sequencing. *Nat. Biotechnol.* **2016**, *34*, 518–524.
[36] Kasianowicz, J. J.; Brandin, E.; Branton, D.; Deamer, D. W. Characterization of individual polynucleotide molecules using a membrane channel. *Proc. Natl. Acad. Sci. USA* **1996**, *93*, 13770–13773.
[37] Loman, N. J.; Quick, J.; Simpson, J. T. A complete bacterial genome assembled *de novo* using only nanopore sequencing data. *Nat. Methods* **2015**, *12*, 733–735.
[38] Stancu, M. C.; van Roosmalen, M. J.; Renkens, I.; Nieboer, M. M.; Middelkamp, S.; de Ligt, J.; Pregno, G.; Giachino, D.; Mandrile, G.; Valle-Inclan, J. E. et al. Mapping and phasing of structural variation in patient genomes using nanopore sequencing. *Nat. Commun.* **2017**, *8*, 1326.
[39] Valle-Inclan, J. E.; Stangl, C.; de Jong, A. C.; van Dessel, L. F.; van Roosmalen, M. J.; Helmijr, J. C. A.; Renkens, I.; de Blank, S.; de Witte, C. J.; Martens, J. W. M. et al. Rapid identification of genomic structural variations with nanopore sequencing enables blood-based cancer monitoring. *MedRxiv*, in press, doi: https://doi.org/10.1101/19011932.
[40] Norris, A. L.; Workman, R. E.; Fan, Y. F.; Eshleman, J. R.; Timp, W. Nanopore sequencing detects structural variants in cancer. *Cancer Biol. Ther.* **2016**, *17*, 246–253.
[41] Minervini, C. F.; Cumbo, C.; Orsini, P.; Brunetti, C.; Anelli, L.; Zagaria, A.; Minervini, A.; Casieri, P.; Coccaro, N.; Tota, G. et al. *TP53* gene mutation analysis in chronic lymphocytic leukemia by nanopore MinION sequencing. *Diagn. Pathol.* **2016**, *11*, 96.
[42] Orsini, P.; Minervini, C. F.; Cumbo, C.; Anelli, L.; Zagaria, A.; Minervini, A.; Coccaro, N.; Tota, G.; Casieri, P.; Impera, L. et al. Design and MinION testing of a nanopore targeted gene sequencing panel for chronic lymphocytic leukemia. *Sci. Rep.* **2018**, *8*, 11798.
[43] Suzuki, A.; Suzuki, M.; Mizushima-Sugano, J.; Frith, M. C.; Makałowski, W.; Kohno, T.; Sugano, S.; Tsuchihara, K.; Suzuki, Y. Sequencing and phasing cancer mutations in lung cancers using a long-read portable sequencer. *DNA Res.* **2017**, *24*, 585–596.
[44] Calin, G. A.; Croce, C. M. MicroRNA signatures in human cancers. *Nat. Rev. Cancer* **2006**, *6*, 857–866.
[45] Mitchell, P. S.; Parkin, R. K.; Kroh, E. M.; Fritz, B. R.; Wyman, S. K.; Pogosova-Agadjanyan, E. L.; Peterson, A.; Noteboom, J.; O' Briant, K. C.; Allen, A. et al. Circulating microRNAs as stable blood-based markers for cancer detection. *Proc. Natl. Acad. Sci. USA* **2008**, *105*, 10513–10518.

[46] Wanunu, M.; Dadosh, T.; Ray, V.; Jin, J. M.; McReynolds, L.; Drndić, M. Rapid electronic detection of probe-specific MicroRNAs using thin nanopore sensors. *Nat. Nanotechnol.* **2010**, *5*, 807–814.

[47] Shim, J.; Kim, Y.; Humphreys, G. I.; Nardulli, A. M.; Kosari, F.; Vasmatzis, G.; Taylor, W. R.; Ahlquist, D. A.; Myong, S.; Bashir, R. Nanopore-based assay for detection of methylation in double-stranded DNA fragments. *ACS Nano* **2015**, *9*, 290–300.

[48] Gilboa, T.; Torfstein, C.; Juhasz, M.; Grunwald, A.; Ebenstein, Y.; Weinhold, E.; Meller, A. Single-molecule DNA methylation quantification using electro-optical sensing in solid-state nanopores. *ACS Nano* **2016**, *10*, 8861–8870.

[49] Wanunu, M.; Cohen-Karni, D.; Johnson, R. R.; Fields, L.; Benner, J.; Peterman, N.; Zheng, Y.; Klein, M. L.; Drndic, M. Discrimination of methylcytosine from hydroxymethylcytosine in DNA molecules. *J. Am. Chem. Soc.* **2011**, *133*, 486–492.

[50] Fologea, D.; Ledden, B.; McNabb, D. S.; Li, J. L. Electrical characterization of protein molecules by a solid-state nanopore. *Appl. Phys. Lett.* **2007**, *91*, 053901.

[51] Yusko, E. C.; Johnson, J. M.; Majd, S.; Prangkio, P.; Rollings, R. C.; Li, J. L.; Yang, J.; Mayer, M. Controlling protein translocation through nanopores with bio-inspired fluid walls. *Nat. Nanotechnol.* **2011**, *6*, 253–260.

[52] Oukhaled, A.; Cressiot, B.; Bacri, L.; Pastoriza-Gallego, M.; Betton, J. M.; Bourhis, E.; Jede, R.; Gierak, J.; Auvray, L.; Pelta, J. Dynamics of completely unfolded and native proteins through solid-state nanopores as a function of electric driving force. *ACS Nano* **2011**, *5*, 3628–3638.

[53] Asandei, A.; Schiopu, I.; Chinappi, M.; Seo, C. H.; Park, Y.; Luchian, T. Electroosmotic trap against the electrophoretic force near a protein nanopore reveals peptide dynamics during capture and translocation. *ACS Appl. Mater. Interfaces* **2016**, *8*, 13166–13179.

[54] Firnkes, M.; Pedone, D.; Knezevic, J.; Döblinger, M.; Rant, U. Electrically facilitated translocations of proteins through silicon nitride nanopores: Conjoint and competitive action of diffusion, electrophoresis, and electroosmosis. *Nano Lett.* **2010**, *10*, 2162–2167.

[55] Sutherland, T. C.; Long, Y. T.; Stefureac, R. I.; Bediako-Amoa, I.; Kraatz, H. B.; Lee, J. S. Structure of peptides investigated by nanopore analysis. *Nano Lett.* **2004**, *4*, 1273–1277.

[56] Giamblanco, N.; Coglitore, D.; Janot, J.-M.; Coulon, P. E.; Charlot, B.; Balme, S. Detection of protein aggregate morphology through single antifouling nanopore. *Sensor. Actuat. B: Chem* **2018**, *260*, 736–745.

[57] Tanimoto, I. M. F.; Cressiot, B.; Jarroux, N.; Roman, J.; Patriarche, G.; Le Pioufle, B.; Pelta, J.; Bacri, L. Selective target protein detection using a decorated nanopore into a microfluidic device. *Biosens. Bioelectron.* **2021**, *183*, 113195.

[58] Thakur, A. K.; Movileanu, L. Single-molecule protein detection in a biofluid using a quantitative nanopore sensor. *ACS Sens.* **2019**, *4*, 2320–2326.

[59] Waduge, P.; Hu, R.; Bandarkar, P.; Yamazaki, H.; Cressiot, B.; Zhao, Q.; Whitford, P. C.; Wanunu, M. Nanopore-based measurements of protein size, fluctuations, and conformational changes. *ACS Nano* **2017**, *11*, 5706–5716.

[60] Kowalczyk, S. W.; Kapinos, L.; Blosser, T. R.; Magalhães, T.; van Nies, P.; Lim, R. Y. H.; Dekker, C. Single-molecule transport across an individual biomimetic nuclear pore complex. *Nat. Nanotechnol.* **2011**, *6*, 433–438.

[61] Rotem, D.; Jayasinghe, L.; Salichou, M.; Bayley, H. Protein detection by nanopores equipped with aptamers. *J. Am. Chem. Soc.* **2012**, *134*, 2781–2787.

[62] Reynaud, L.; Bouchet-Spinelli, A.; Janot, J. M.; Buhot, A.; Balme, S.; Raillon, C. Discrimination of α-thrombin and γ-thrombin using aptamer-functionalized nanopore sensing. *Anal. Chem.* **2021**, *93*, 7889–7897.

[63] Jia, W. D.; Hu, C. Z.; Wang, Y. Q.; Gu, Y. M.; Qian, G. R.; Du, X. Y.; Wang, L. Y.; Liu, Y.; Cao, J.; Zhang, S. Y. et al. Programmable nano-reactors for stochastic sensing. *Nat. Commun.* **2021**, *12*, 5811.

[64] Sze, J. Y. Y.; Ivanov, A. P.; Cass, A. E. G.; Edel, J. B. Single molecule multiplexed nanopore protein screening in human serum using aptamer modified DNA carriers. *Nat. Commun.* **2017**, *8*, 1552.

[65] Lucas, F. L. R.; Sarthak, K.; Lenting, E. M.; Coltan, D.; van der Heide, N. J.; Versloot, R. C. A.; Aksimentiev, A.; Maglia, G. The manipulation of the internal hydrophobicity of FraC nanopores augments peptide capture and recognition. *ACS Nano* **2021**, *15*, 9600–9613.

[66] Zernia, S.; van der Heide, N. J.; Galenkamp, N. S.; Gouridis, G.; Maglia, G. Current blockades of proteins inside nanopores for real-time metabolome analysis. *ACS Nano* **2020**, *14*, 2296–2307.

[67] Biomarkers and surrogate endpoints: Preferred definitions and conceptual framework. *Clin. Pharmacol. Ther.* **2001**, *69*, 89–95.

[68] Lin, Y.; Ying, Y. L.; Shi, X.; Liu, S. C.; Long, Y. T. Direct sensing of cancer biomarkers in clinical samples with a designed nanopore. *Chem. Commun.* **2017**, *53*, 11564–11567.

[69] Greninger, A. L.; Naccache, S. N.; Federman, S.; Yu, G. X.; Mbala, P.; Bres, V.; Stryke, D.; Bouquet, J.; Somasekar, S.; Linnen, J. M. et al. Rapid metagenomic identification of viral pathogens in clinical samples by real-time nanopore sequencing analysis. *Genome Med.* **2015**, *7*, 99.

[70] Xu, Y. F.; Lewandowski, K.; Jeffery, K.; Downs, L. O.; Foster, D.; Sanderson, N. D.; Kavanagh, J.; Vaughan, A.; Salvagno, C.; Vipond, R. et al. Nanopore metagenomic sequencing to investigate nosocomial transmission of human metapneumovirus from a unique genetic group among haematology patients in the united kingdom. *J. Infect.* **2020**, *80*, 571–577.

[71] Lewandowski, K.; Xu, Y. F.; Pullan, S. T.; Lumley, S. F.; Foster, D.; Sanderson, N.; Vaughan, A.; Morgan, M.; Bright, N.; Kavanagh, J. et al. Metagenomic nanopore sequencing of influenza virus direct from clinical respiratory samples. *J. Clin. Microbiol.* **2019**, *58*, e00963–19.

[72] Kafetzopoulou, L. E.; Pullan, S. T.; Lemey, P.; Suchard, M. A.; Ehichioya, D. U.; Pahlmann, M.; Thielebein, A.; Hinzmann, J.; Oestereich, L.; Wozniak, D. M. et al. Metagenomic sequencing at the epicenter of the Nigeria 2018 Lassa fever outbreak. *Science* **2019**, *363*, 74–77.

[73] Wang, M.; Fu, A. S.; Hu, B.; Tong, Y. Q.; Liu, R.; Liu, Z.; Gu, J. S.; Xiang, B.; Liu, J. H.; Jiang, W. et al. Nanopore targeted sequencing for the accurate and comprehensive detection of SARS-CoV-2 and other respiratory viruses. *Small* **2020**, *16*, 2002169.

[74] Keita, A. K.; Koundouno, F. R.; Faye, M.; Düx, A.; Hinzmann, J.; Diallo, H.; Ayouba, A.; Le Marcis, F.; Soropogui, B.; Ifono, K. et al. Resurgence of Ebola virus in 2021 in guinea suggests a new paradigm for outbreaks. *Nature* **2021**, *597*, 539–543.

[75] Oxford Nanopore Technologies. *200 Oxford Nanopore Sequencers Have Left Uk for China, to Support Rapid, Near-Sample Coronavirus Sequencing for Outbreak Surveillance* [Online]. Oxford Nanopore Technologies: Oxford, 2020. https://nanoporetech.com/about-us/news/200-oxford-nanopore-sequencers-have-left-uk-china-support-rapid-near-sample (accessed Jan 29, 2022).

[76] Tang, Z. F. ; Nouri, R. ; Dong, M. ; Yang, J. B. ; Greene, W. ; Zhu, Y. S. ; Yon, M. ; Nair, M. S. ; Kuchipudi, S. V. ; Guan, W. H. Rapid detection of novel coronavirus SARS-CoV-2 by RT-LAMP coupled solid-state nanopores. *Biosens. Bioelectron.* **2022**, *197*, 113759.

[77] Bull, R. A.; Adikari, T. N.; Ferguson, J. M.; Hammond, J. M.; Stevanovski, I.; Beukers, A. G.; Naing, Z.; Yeang, M.; Verich, A.; Gamaarachchi, H. et al. Analytical validity of nanopore sequencing for rapid SARS-CoV-2 genome analysis. *Nat. Commun.* **2020**, *11*, 6272.

[78] Li, J.; Wang, H. Q.; Mao, L. F.; Yu, H.; Yu, X. F.; Sun, Z.; Qian, X.; Cheng, S.; Chen, S. C.; Chen, J. F. et al. Rapid genomic characterization of SARS-CoV-2 viruses from clinical specimens using nanopore sequencing. *Sci. Rep.* **2020**, *10*, 17492.

[79] Munnink, B. B. O.; Nieuwenhuijse, D. F.; Stein, M.; O'Toole, Á.; Haverkate, M.; Mollers, M.; Kamga, S. K.; Schapendonk, C.; Pronk, M.; Lexmond, P. et al. Rapid SARS-CoV-2 whole-genome sequencing and analysis for informed public health decision-making in the Netherlands. *Nat. Med.* **2020**, *26*, 1405–1410.

[80] Tegally, H.; Wilkinson, E.; Giovanetti, M.; Iranzadeh, A.; Fonseca, V.; Giandhari, J.; Doolabh, D.; Pillay, S.; San, E. J.; Msomi, N. et al. Detection of a SARS-CoV-2 variant of concern in south Africa. *Nature* **2021**, *592*, 438–443.

[81] Arima, A.; Tsutsui, M.; Yoshida, T.; Tatematsu, K.; Yamazaki, T.; Yokota, K.; Kuroda, S.; Washio, T.; Baba, Y.; Kawai, T. Digital pathology platform for respiratory tract infection diagnosis via multiplex single-particle detections. *ACS Sens.* **2020**, *5*, 3398–3403.

[82] Arima, A.; Tsutsui, M.; Harlisa, I. H.; Yoshida, T.; Tanaka, M.; Yokota, K.; Tonomura, W.; Taniguchi, M.; Okochi, M.; Washio, T. et al. Selective detections of single-viruses using solid-state nanopores. *Sci. Rep.* **2018**, *8*, 16305.

[83] Arima, A.; Tsutsui, M.; Washio, T.; Baba, Y.; Kawai, T. Solid-state nanopore platform integrated with machine learning for digital diagnosis of virus infection. *Anal. Chem.* **2021**, *93*, 215–227.

[84] Gu, L. Q.; Braha, O.; Conlan, S.; Cheley, S.; Bayley, H. Stochastic sensing of organic analytes by a pore-forming protein containing a molecular adapter. *Nature* **1999**, *398*, 686–690.

[85] Wu, H. C.; Bayley, H. Single-molecule detection of nitrogen mustards by covalent reaction within a protein nanopore. *J. Am. Chem. Soc.* **2008**, *130*, 6813–6819.

[86] Prajapati, J. D.; Kleinekathöfer, U.; Winterhalter, M. How to enter a bacterium: Bacterial porins and the permeation of antibiotics. *Chem. Rev.* **2021**, *121*, 5158–5192.

[87] Li, F. M.; Liang, Z.; Zheng, X.; Zhao, W.; Wu, M.; Wang, Z. Y. Toxicity of nano-TiO_2 on algae and the site of reactive oxygen species production. *Aquat. Toxicol.* **2015**, *158*, 1–13.

[88] Schaumann, G. E.; Philippe, A.; Bundschuh, M.; Metreveli, G.; Klitzke, S.; Rakcheev, D.; Grün, A.; Kumahor, S. K.; Kühn, M.; Baumann, T. et al. Understanding the fate and biological effects of Ag- and TiO_2-nanoparticles in the environment: The quest for advanced analytics and interdisciplinary concepts. *Sci. Total Environ.* **2015**, *535*, 3–19.

[89] Book, F.; Backhaus, T. Aquatic ecotoxicity of manufactured silica nanoparticles: A systematic review and meta-analysis. *Sci. Total Environ.* **2022**, *806*, 150893.

[90] Chen, L. J.; Liu, J.; Zhang, Y. L.; Zhang, G. L.; Kang, Y. Y.; Chen, A. J.; Feng, X. L.; Shao, L. Q. The toxicity of silica nanoparticles to the immune system. *Nanomedicine* **2018**, *13*, 1939–1962.

[91] Zhang, C. Q.; Hu, Z. Q.; Deng, B. L. Silver nanoparticles in aquatic environments: Physiochemical behavior and antimicrobial mechanisms. *Water Res.* **2016**, *88*, 403–427.

[92] McGillicuddy, E.; Murray, I.; Kavanagh, S.; Morrison, L.; Fogarty, A.; Cormican, M.; Dockery, P.; Prendergast, M.; Rowan, N.; Morris, D. Silver nanoparticles in the environment: Sources, detection and ecotoxicology. *Sci. Total Environ.* **2017**, *575*, 231–246.

[93] Zhang, W. C.; Xiao, B. D.; Fang, T. Chemical transformation of silver nanoparticles in aquatic environments: Mechanism, morphology and toxicity. *Chemosphere* **2018**, *191*, 324–334.

[94] Andrady, A. L. Microplastics in the marine environment. *Mar. Pollut. Bull.* **2011**, *62*, 1596–1605.

[95] Horton, A. A.; Walton, A.; Spurgeon, D. J.; Lahive, E.; Svendsen, C. Microplastics in freshwater and terrestrial environments: Evaluating the current understanding to identify the knowledge gaps and future research priorities. *Sci. Total Environ.* **2017**, *586*, 127–141.

[96] *Titanium Dioxide Market by Grade* (*Rutile*, *Anatase*), *Process* (*Sulfate*, *Chloride*), *Application* (*Paints & Coating*, *Plastics*, *Paper*, *Inks*), *& Region* (*North America*, *Europe*, *Asia Pacific*, *MEA*, *South America*)-*Trends and Forecasts up to 2026* [Online]. 2021. https://www.researchandmarkets.com/reports/5359990/titanium-dioxide-market-by-grade-rutile#src-pos-2 (accessed Jan 26, 2022).

[97] Reports and Data. *Silicon Dioxide Market* [Online]. Marketysers Global Consulting LLP, 2020. https://www.reportsanddata.com/report-detail/silicon-dioxide-market (accessed Jan 26, 2022).

[98] Ahuja, K. ; Rawat, A. *Silver Nanoparticles Market Size and Share* [Online]. Global Market Insights: Selbyville, 2020. https://www.gminsights.com/industry-analysis/silver-nanoparticles-market (accessed Jan 26, 2022).

[99] Bacri, L.; Oukhaled, A. G.; Schiedt, B.; Patriarche, G.; Bourhis, E.; Gierak, J.; Pelta, J.; Auvray, L. Dynamics of colloids in single solid-state nanopores. *J. Phys. Chem. B* **2011**, *115*, 2890–2898.

[100] Tsutsui, M.; Yokota, K.; Yoshida, T.; Hotehama, C.; Kowada, H.; Esaki, Y.; Taniguchi, M.; Washio, T.; Kawai, T. Identifying single particles in air using a 3D-integrated solid-state pore. *ACS Sens.* **2019**, *4*, 748–755.

[101] Kangasluoma, J.; Attoui, M. Review of Sub-3 Nm condensation particle counters, calibrations, and cluster generation methods. *Aerosol Sci. Technol.* **2019**, *53*, 1277–1310.

[102] Ploetz, E.; Engelke, H.; Lächelt, U.; Wuttke, S. The chemistry of reticular framework nanoparticles: MOF, ZIF, and COF materials. *Adv. Funct. Mater.* **2020**, *30*, 1909062.

[103] Christoff-Tempesta, T.; Cho, Y.; Kim, D. Y.; Geri, M.; Lamour, G.; Lew, A. J.; Zuo, X. B.; Lindemann, W. R.; Ortony, J. H. Self-assembly of aramid amphiphiles into ultra-stable nanoribbons and aligned nanoribbon threads. *Nat. Nanotechnol.* **2021**, *16*, 447–454.

[104] Butt, H. J. Electrostatic interaction in atomic force microscopy. *Biophys. J.* **1991**, *60*, 777–785.

[105] Lamour, G.; Allard, A.; Pelta, J.; Labdi, S.; Lenz, M.; Campillo, C. Mapping and modeling the nanomechanics of bare and protein-coated lipid nanotubes. *Phys. Rev. X* **2020**, *10*, 011031.

[106] Carney, R. P.; Astier, Y.; Carney, T. M.; Voïtchovsky, K.; Silva, P. H. J.; Stellacci, F. Electrical method to quantify nanoparticle interaction with lipid bilayers. *ACS Nano* **2013**, *7*, 932–942.

[107] Langevin, D.; Raspaud, E.; Mariot, S.; Knyazev, A.; Stocco, A.; Salonen, A.; Luch, A.; Haase, A.; Trouiller, B.; Relier, C. et al. Towards reproducible measurement of nanoparticle size using dynamic light scattering: Important controls and considerations. *NanoImpact* **2018**, *10*, 161–167.

[108] DeBlois, R. W.; Bean, C. P. Counting and sizing of submicron particles by the resistive pulse technique. *Rev. Sci. Instrum.* **1970**, *41*, 909–916.

[109] Cabello-Aguilar, S.; Chaaya, A. A.; Bechelany, M.; Pochat-Bohatier, C.; Balanzat, E.; Janot, J. M.; Miele, P.; Balme, S. Dynamics of polymer nanoparticles through a single artificial nanopore with a high-aspect-ratio. *Soft Matter* **2014**, *10*, 8413–8419.

[110] Ito, T.; Sun, L.; Bevan, M. A.; Crooks, R. M. Comparison of nanoparticle size and electrophoretic mobility measurements using a carbon-nanotube-based coulter counter, dynamic light scattering, transmission electron microscopy, and phase analysis light scattering. *Langmuir* **2004**, *20*, 6940–6945.

[111] Petrossian, L.; Wilk, S. J.; Joshi, P.; Goodnick, S. M.; Thornton, T. J. Demonstration of coulter counting through a cylindrical solid state nanopore. *J. Phys.: Conf. Ser.* **2008**, *109*, 012028.

[112] Arjmandi, N.; van Roy, W.; Lagae, L. Measuring mass of nanoparticles and viruses in liquids with nanometer-scale pores. *Anal. Chem.* **2014**, *86*, 4637–4641.

[113] Tsutsui, M.; Hongo, S.; He, Y. H.; Taniguchi, M.; Gemma, N.; Kawai, T. Single-nanoparticle detection using a low-aspect-ratio pore. *ACS Nano* **2012**, *6*, 3499–3505.

[114] Liu, S.; Zhao, Y.; Parks, J. W.; Deamer, D. W.; Hawkins, A. R.; Schmidt, H. Correlated electrical and optical analysis of single nanoparticles and biomolecules on a nanopore-gated optofluidic chip. *Nano Lett.* **2014**, *14*, 4816–4820.

[115] Roman, J.; Jarroux, N.; Patriarche, G.; Français, O.; Pelta, J.; Le Pioufle, B.; Bacri, L. Functionalized solid-state nanopore integrated in a reusable microfluidic device for a better stability and nanoparticle detection. *ACS Appl. Mater. Interfaces* **2017**, *9*, 41634–41640.

[116] Coglitore, D.; Merenda, A.; Giamblanco, N.; Dumée, L. F.; Janot, J. M.; Balme, S. Metal alloy solid-state nanopores for single nanoparticle detection. *Phys. Chem. Chem. Phys.* **2018**, *20*, 12799–12807.

[117] Davenport, M.; Healy, K.; Pevarnik, M.; Teslich, N.; Cabrini, S.; Morrison, A. P.; Siwy, Z. S.; Létant, S. E. The role of pore geometry in single nanoparticle detection. *ACS Nano* **2012**, *6*, 8366–8380.

[118] Gadaleta, A.; Biance, A. L.; Siria, A.; Bocquet, L. Ultra-sensitive

flow measurement in individual nanopores through pressure-driven particle translocation. *Nanoscale* **2015**, *7*, 7965–7970.
[119] Balme, S.; Lepoitevin, M.; Dumé, L. F.; Bechelany, M.; Janot, J. M. Diffusion dynamics of latex nanoparticles coated with SsDNA across a single nanopore. *Soft Matter* **2017**, *13*, 496–502.
[120] Cao, Y.; Lin, Y.; Qian, R. C.; Ying, Y. L.; Si, W.; Sha, J. J.; Chen, Y. F.; Long, Y. T. Evidence of single-nanoparticle translocation through a solid-state nanopore by plasmon resonance energy transfer. *Chem. Commun.* **2016**, *52*, 5230–5233.
[121] Tan, S. W.; Wang, L.; Liu, H.; Wu, H. W.; Liu, Q. J. Single nanoparticle translocation through chemically modified solid nanopore. *Nanoscale Res. Lett.* **2016**, *11*, 50.
[122] Darvish, A.; Goyal, G.; Aneja, R.; Sundaram, R. V. K.; Lee, K.; Ahn, C. W.; Kim, K. B.; Vlahovska, P. M.; Kim, M. J. Nanoparticle mechanics: Deformation detection via nanopore resistive pulse sensing. *Nanoscale* **2016**, *8*, 14420–14431.
[123] Venta, K. E.; Zanjani, M. B.; Ye, X. C.; Danda, G.; Murray, C. B.; Lukes, J. R.; Drndić, M. Gold nanorod translocations and charge measurement through solid-state nanopores. *Nano Lett.* **2014**, *14*, 5358–5364.
[124] Lan, W. J.; White, H. S. Diffusional motion of a particle translocating through a nanopore. *ACS Nano* **2012**, *6*, 1757–1765.
[125] Meyer, N.; Janot, J. M.; Lepoitevin, M.; Smietana, M.; Vasseur, J. J.; Torrent, J.; Balme, S. Machine learning to improve the sensing of biomolecules by conical track-etched nanopore. *Biosensors* **2020**, *10*, 140.
[126] Fu, J. Y.; Wu, L. L.; Qiao, Y.; Tu, J.; Lu, Z. H. Microfluidic systems applied in solid-state nanopore sensors. *Micromachines* **2020**, *11*, 332.
[127] Kang, X. F.; Cheley, S.; Rice-Ficht, A. C.; Bayley, H. A storable encapsulated bilayer chip containing a single protein nanopore. *J. Am. Chem. Soc.* **2007**, *129*, 4701–4705.
[128] Kannan, N.; Vakeesan, D. Solar energy for future world: A review. *Renewable Sustainable Energy Rev.* **2016**, *62*, 1092–1105.
[129] Wang, Z. M.; Liu, W. M. Wind energy potential assessment based on wind speed, its direction and power data. *Sci. Rep.* **2021**, *11*, 16879.
[130] Barthelmie, R. J.; Pryor, S. C. Potential contribution of wind energy to climate change mitigation. *Nat. Climate Change* **2014**, *4*, 684–688.
[131] Zhang, L. X.; Liu, Z. H.; Cui, G. L.; Chen, L. Q. Biomass-derived materials for electrochemical energy storages. *Prog. Polym. Sci.* **2015**, *43*, 136–164.
[132] Jolie, E.; Scott, S.; Faulds, J.; Chambefort, I.; Axelsson, G.; Gutiérrez-Negrín, L. C.; Regenspurg, S.; Ziegler, M.; Ayling, B.; Richter, A. et al. Geological controls on geothermal resources for power generation. *Nat. Rev. Earth Environ.* **2021**, *2*, 324–339.
[133] Hsu, J. P.; Su, T. C.; Lin, C. Y.; Tseng, S. Power generation from a pH-regulated nanochannel through reverse electrodialysis: Effects of nanochannel shape and non-uniform H^+ distribution. *Electrochim. Acta* **2019**, *294*, 84–92.
[134] Tseng, S.; Li, Y. M.; Lin, C. Y.; Hsu, J. P. Salinity gradient power: Optimization of nanopore size. *Electrochim. Acta* **2016**, *219*, 790–797.
[135] Post, J. W.; Hamelers, H. V. M.; Buisman, C. J. N. Energy recovery from controlled mixing salt and fresh water with a reverse electrodialysis system. *Environ. Sci. Technol.* **2008**, *42*, 5785–5790.
[136] Wang, Z. X.; Wang, L.; Elimelech, M. Viability of harvesting salinity gradient (blue) energy by nanopore-based osmotic power generation. *Engineering* **2022**, *9*, 51–60.
[137] Logan, B. E.; Elimelech, M. Membrane-based processes for sustainable power generation using water. *Nature* **2012**, *488*, 313–319.
[138] Helfer, F.; Lemckert, C.; Anissimov, Y. G. Osmotic power with pressure retarded osmosis: Theory, performance and trends-a review. *J. Memb. Sci.* **2014**, *453*, 337–358.
[139] Yip, N. Y.; Elimelech, M. Thermodynamic and energy efficiency analysis of power generation from natural salinity gradients by pressure retarded osmosis. *Environ. Sci. Technol.* **2012**, *46*, 5230–5239.
[140] Yip, N. Y.; Vermaas, D. A.; Nijmeijer, K.; Elimelech, M. Thermodynamic, energy efficiency, and power density analysis of reverse electrodialysis power generation with natural salinity gradients. *Environ. Sci. Technol.* **2014**, *48*, 4925–4936.
[141] Kim, J.; Kim, S. J.; Kim, D. K. Energy harvesting from salinity gradient by reverse electrodialysis with anodic alumina nanopores. *Energy* **2013**, *51*, 413–421.
[142] Hong, J. G.; Zhang, B. P.; Glabman, S.; Uzal, N.; Dou, X. M.; Zhang, H. G.; Wei, X. Z.; Chen, Y. S. Potential ion exchange membranes and system performance in reverse electrodialysis for power generation: A review. *J. Memb. Sci.* **2015**, *486*, 71–88.
[143] Straub, A. P.; Deshmukh, A.; Elimelech, M. Pressure-retarded osmosis for power generation from salinity gradients: Is it viable. *Energy Environ. Sci.* **2016**, *9*, 31–48.
[144] Yip, N. Y.; Brogioli, D.; Hamelers, H. V. M.; Nijmeijer, K. Salinity gradients for sustainable energy: Primer, progress, and prospects. *Environ. Sci. Technol.* **2016**, *50*, 12072–12094.
[145] Nijmeijer, K.; Metz, S. Chapter 5 salinity gradient energy. *Sustain. Sci. Eng.* **2010**, *2*, 95–139.
[146] Siria, A.; Bocquet, M. L.; Bocquet, L. New avenues for the large-scale harvesting of blue energy. *Nat. Rev. Chem.* **2017**, *1*, 0091.
[147] Graf, M.; Lihter, M.; Unuchek, D.; Sarathy, A.; Leburton, J. P.; Kis, A.; Radenovic, A. Light-enhanced blue energy generation using MoS_2 nanopores. *Joule* **2019**, *3*, 1549–1564.
[148] Siria, A.; Poncharal, P.; Biance, A. L.; Fulcrand, R.; Blase, X.; Purcell, S. T.; Bocquet, L. Giant osmotic energy conversion measured in a single transmembrane boron nitride nanotube. *Nature* **2013**, *494*, 455–458.
[149] Macha, M.; Marion, S.; Nandigana, V. V. R.; Radenovic, A. 2D materials as an emerging platform for nanopore-based power generation. *Nat. Rev. Mater.* **2019**, *4*, 588–605.
[150] Liu, X.; He, M.; Calvani, D.; Qi, H. Y.; Gupta, K. B. S. S.; de Groot, H. J. M.; Sevink, G. J. A.; Buda, F.; Kaiser, U.; Schneider, G. F. Power generation by reverse electrodialysis in a single-layer nanoporous membrane made from core-rim polycyclic aromatic hydrocarbons. *Nat. Nanotechnol.* **2020**, *15*, 307–312.
[151] Choi, J. W.; Aurbach, D. Promise and reality of post-lithium-ion batteries with high energy densities. *Nat. Rev. Mater.* **2016**, *1*, 16013.
[152] Goodenough, J. B.; Park, K. S. The Li-ion rechargeable battery: A perspective. *J. Am. Chem. Soc.* **2013**, *135*, 1167–1176.
[153] Vegge, T.; Tarascon, J. M.; Edström, K. Toward better and smarter batteries by combining AI with multisensory and self-healing approaches. *Adv. Energy Mater.* **2021**, *11*, 2100362.
[154] Narayan, R. ; Laberty-Robert, C. ; Pelta, J. ; Tarascon, J. M. ; Dominko, R. Self-healing: An emerging technology for next-generation smart batteries. *Adv. Energy Mater.*, in press, https://doi.org/10.1002/aenm.202102652.
[155] Dunn, B.; Kamath, H.; Tarascon, J. M. Electrical energy storage for the grid: A battery of choices. *Science* **2011**, *334*, 928–935.
[156] Vizintin, A.; Lozinšek, M.; Chellappan, R. K.; Foix, D.; Krajnc, A.; Mali, G.; Drazic, G.; Genorio, B.; Dedryvère, R.; Dominko, R. Fluorinated reduced graphene oxide as an interlayer in Li-S batteries. *Chem. Mater.* **2015**, *27*, 7070–7081.
[157] Busche, M. R.; Adelhelm, P.; Sommer, H.; Schneider, H.; Leitner, K.; Janek, J. Systematical electrochemical study on the parasitic shuttle-effect in lithium-sulfur-cells at different temperatures and different rates. *J. Power Sources* **2014**, *259*, 289–299.
[158] Grey, C. P.; Tarascon, J. M. Sustainability and *in situ* monitoring in battery development. *Nat. Mater.* **2017**, *16*, 45–56.
[159] Patel, M. U. M.; Demir-Cakan, R.; Morcrette, M.; Tarascon, J. M.; Gaberscek, M.; Dominko, R. Li-S battery analyzed by UV/Vis in operando mode. *ChemSusChem* **2013**, *6*, 1177–1181.
[160] Hua, X.; Zhang, T.; Offer, G. J.; Marinescu, M. Towards online tracking of the shuttle effect in lithium sulfur batteries using differential thermal voltammetry. *J. Energy Storage* **2019**, *21*, 765–772.
[161] Sathiya, M.; Leriche, J. B.; Salager, E.; Gourier, D.; Tarascon, J. M.; Vezin, H. Electron paramagnetic resonance imaging for real-time monitoring of Li-ion batteries. *Nat. Commun.* **2015**, *6*, 6276.
[162] Lin, F.; Liu, Y. J.; Yu, X. Q.; Cheng, L.; Singer, A.; Shpyrko, O. G.; Xin, H. L.; Tamura, N.; Tian, C. X.; Weng, T. C. et al.

Synchrotron X-ray analytical techniques for studying materials electrochemistry in rechargeable batteries. *Chem. Rev.* **2017**, *117*, 13123–13186.

[163] Zheng, D.; Qu, D. Y.; Yang, X. Q.; Yu, X. Q.; Lee, H. S.; Qu, D. Y. Quantitative and qualitative determination of polysulfide species in the electrolyte of a lithium-sulfur battery using HPLC ESI/MS with one-step derivatization. *Adv. Energy Mater.* **2015**, *5*, 140188.

[164] Huang, J. Q.; Blanquer, L. A.; Bonefacino, J.; Logan, E. R.; Corte, D. A. D.; Delacourt, C.; Gallant, B. M.; Boles, S. T.; Dahn, J. R.; Tam, H. Y. et al. Operando decoding of chemical and thermal events in commercial Na(Li)-ion cells via optical sensors. *Nat. Energy* **2020**, *5*, 674–683.

[165] Huang, J. Q.; Han, X. L.; Liu, F.; Gervillié, C.; Blanquer, L. A.; Guo, T.; Tarascon, J. M. Monitoring battery electrolyte chemistry via *in-operando* tilted fiber Bragg grating sensors. *Energy Environ. Sci.* **2021**, *14*, 6464–6475.

[166] Bétermier, F.; Cressiot, B.; Di Muccio, G.; Jarroux, N.; Bacri, L.; Rocca, B. M. D.; Chinappi, M.; Pelta, J.; Tarascon, J. M. Single-sulfur atom discrimination of polysulfides with a protein nanopore for improved batteries. *Commun. Mater.* **2020**, *1*, 59.

[167] Meier, W.; Nardin, C.; Winterhalter, M. Reconstitution of channel proteins in (polymerized) ABA triblock copolymer membranes. *Angew. Chem., Int. Ed.* **2000**, *39*, 4599–4602.

[168] Ma, T. J.; Janot, J. M.; Balme, S. Track-etched nanopore/membrane: From fundamental to applications. *Small Methods* **2020**, *4*, 2000366.

[169] Hall, A. R.; Scott, A.; Rotem, D.; Mehta, K. K.; Bayley, H.; Dekker, C. Hybrid pore formation by directed insertion of α-haemolysin into solid-state nanopores. *Nat. Nanotechnol.* **2010**, *5*, 874–877.

[170] Cabello-Aguilar, S.; Balme, S.; Chaaya, A. A.; Bechelany, M.; Balanzat, E.; Janot, J. M.; Pochat-Bohatier, C.; Miele, P.; Dejardin, P. Slow translocation of polynucleotides and their discrimination by α-hemolysin inside a single track-etched nanopore designed by atomic layer deposition. *Nanoscale* **2013**, *5*, 9582–9586.

[171] Cressiot, B.; Greive, S. J.; Mojtabavi, M.; Antson, A. A.; Wanunu, M. Thermostable virus portal proteins as reprogrammable adapters for solid-state nanopore sensors. *Nat. Commun.* **2018**, *9*, 4652.

[172] Lee, P. L. J.; Thangavel, V.; Guery, C.; Trautmann, C.; Toimil-Molares, M. E.; Morcrette, M. Etched ion-track membranes as tailored separators in Li-S batteries. *Nanotechnology* **2021**, *32*, 365401.

[173] Liu, Y. X.; Kearney, J.; Mahmoud, M.; Kille, B.; Sedlazeck, F. J.; Treangen, T. J. Rescuing low frequency variants within intra-host viral populations directly from Oxford Nanopore sequencing data. *Nat. Commun.* **2022**, *13*, 1321.

[174] Cressiot, B.; Bacri, L.; Pelta, J. The promise of nanopore technology: Advances in the discrimination of protein sequences and chemical modifications. *Small Methods* **2020**, *4*, 2000090.

[175] Restrepo-Pérez, L.; Joo, C.; Dekker, C. Paving the way to single-molecule protein sequencing. *Nat. Nanotechnol.* **2018**, *13*, 786–796.

[176] Ouldali, H.; Sarthak, K.; Ensslen, T.; Piguet, F.; Manivet, P.; Pelta, J.; Behrends, J. C.; Aksimentiev, A.; Oukhaled, A. Electrical recognition of the twenty proteinogenic amino acids using an aerolysin nanopore. *Nat. Biotechnol.* **2020**, *38*, 176–181.

[177] Piguet, F.; Ouldali, H.; Pastoriza-Gallego, M.; Manivet, P.; Pelta, J.; Oukhaled, A. Identification of single amino acid differences in uniformly charged homopolymeric peptides with aerolysin nanopore. *Nat. Commun.* **2018**, *9*, 966.

[178] Asandei, A.; Rossini, A. E.; Chinappi, M.; Park, Y.; Luchian, T. Protein nanopore-based discrimination between selected neutral amino acids from polypeptides. *Langmuir* **2017**, *33*, 14451–14459.

[179] Huang, G.; Voet, A.; Maglia, G. FraC nanopores with adjustable diameter identify the mass of opposite-charge peptides with 44 dalton resolution. *Nat. Commun.* **2019**, *10*, 835.

[180] Rosen, C. B.; Rodriguez-Larrea, D.; Bayley, H. Single-molecule site-specific detection of protein phosphorylation with a nanopore. *Nat. Biotechnol.* **2014**, *32*, 179–181.

[181] Restrepo-Pérez, L.; Huang, G.; Bohländer, P. R.; Worp, N.; Eelkema, R.; Maglia, G.; Joo, C.; Dekker, C. Resolving chemical modifications to a single amino acid within a peptide using a biological nanopore. *ACS Nano* **2019**, *13*, 13668–13676.

[182] Restrepo-Pérez, L.; Wong, C. H.; Maglia, G.; Dekker, C.; Joo, C. Label-free detection of post-translational modifications with a nanopore. *Nano Lett.* **2019**, *19*, 7957–7964.

[183] Ying, Y. L.; Yang, J.; Meng, F. N.; Li, S.; Li, M. Y.; Long, Y. T. A nanopore phosphorylation sensor for single oligonucleotides and peptides. *Research* **2019**, *2019*, 1050735.

[184] Lucas, F. L. R.; Versloot, R. C. A.; Yakovlieva, L.; Walvoort, M. T. C.; Maglia, G. Protein identification by nanopore peptide profiling. *Nat. Commun.* **2021**, *12*, 5795.

[185] Brinkerhoff, H.; Kang, A. S. W.; Liu, J. Q.; Aksimentiev, A.; Dekker, C. Multiple rereads of single proteins at single-amino acid resolution using nanopores. *Science* **2021**, *374*, 1509–1513.

[186] Yan, S. H.; Zhang, J. Y.; Wang, Y.; Guo, W. M.; Zhang, S. Y.; Liu, Y.; Cao, J.; Wang, Y. Q.; Wang, L. Y.; Ma, F. B. et al. Single molecule ratcheting motion of peptides in a *Mycobacterium smegmatis* porin A (MspA) nanopore. *Nano Lett.* **2021**, *21*, 6703–6710.

[187] Chen, Z. J.; Wang, Z. Q.; Xu, Y.; Zhang, X. C.; Tian, B. X.; Bai, J. W. Controlled movement of SsDNA conjugated peptide through *Mycobacterium Smegmatis* porin A (MspA) nanopore by a helicase motor for peptide sequencing application. *Chem. Sci.* **2021**, *12*, 15750–15756.

[188] Wang, H. Y.; Ying, Y. L.; Li, Y.; Kraatz, H. B.; Long, Y. T. Nanopore analysis of β-amyloid peptide aggregation transition induced by small molecules. *Anal. Chem.* **2011**, *83*, 1746–1752.

[189] Meyer, N.; Arroyo, N.; Janot, J. M.; Lepoitevin, M.; Stevenson, A.; Nemeir, I. A.; Perrier, V.; Bougard, D.; Belondrade, M.; Cot, D. et al. Detection of amyloid-β fibrils using track-etched nanopores: Effect of geometry and crowding. *ACS Sens.* **2021**, *6*, 3733–3743.

[190] Meyer, N.; Arroyo, N.; Baldelli, M.; Coquart, N.; Janot, J. M.; Perrier, V.; Chinappi, M.; Picaud, F.; Torrent, J.; Balme, S. Conical nanopores highlight the pro-aggregating effects of pyrimethanil fungicide on Aβ(1-42) peptides and dimeric splitting phenomena. *Chemosphere* **2022**, *291*, 132733.